ROLES OF TBP N-TERMINUS IN 3D GENOME ORGANIZATION AND GENE REGULATION

by

BRITTNEY LEE

A THESIS

Presented to the Department of Biology and Human Physiology
and the Robert D. Clark Honors College
in partial fulfillment of the requirements for the degree of
Bachelor of Science

May 2024

An Abstract of the Thesis of

Brittney Lee for the degree of Science
in the Department of Biology to be taken June, 2024

Title: Roles of TBP N-Terminus on 3D Genome Organization and Gene Regulation

Approved: *Ken-ichi Noma Ph.D.*
Primary Thesis Advisor

Recent studies have underscored the pivotal roles of transcription factors, such as the TATA-box binding protein (TBP), in governing gene expression dynamics by regulating the transcription process from DNA to RNA. Particular attention has been drawn to the multifaceted functionalities of the TBP N-terminus in transcriptional control and the structural organization of the genome in three dimensions. Investigations, notably utilizing fission yeast models, have elucidated its participation in coordinating responses to stress, ensuring proper gene distribution during cell division, and facilitating the establishment of gene territories via phase separation phenomena. Manipulation of the TBP N-terminus has yielded valuable insights into its contributions to transcriptional activity, cellular homeostasis, and genomic architecture under stress conditions, offering pertinent implications for comprehending fundamental cellular processes and potential mechanisms of disease, such as cancer. This thesis demonstrates that alterations to the TBP N-terminus impair both cell growth, as evidenced by spot tests and doubling time assays, and the overall organization of DNA, as observed through microscopic examination of TBP-N terminal mutants under various culturing conditions. Leveraging next-generation sequencing (NGS) technology, I reveal a widespread dampening of gene expression in TBP N-terminal mutants, albeit with no significant alterations in protein binding distribution overall.

Based on these observations, I posit that the TBP N-terminus plays a pivotal role in facilitating appropriate stress responses in fission yeast cells, thereby ensuring the accurate segregation of transcribed genes alongside their expression levels and spatial localization within the genome.

Acknowledgements

I would like to thank Dr. Ken-ichi Noma for his tremendous support and exceptional guidance during the past two and a half years since I've been a part of the Noma Lab. Dr. Noma's invaluable insights, encouragement, and expertise have been instrumental in advancing my research and professional development. Dr. Noma has always been so dedicated to fostering a collaborative and innovative environment, which has greatly enriched my lab experience, and I am truly grateful for the opportunity to work on projects under the Noma Lab. I would also like to express my gratitude to Dr. Sanki Tashiro for being the best mentor I could ever ask for. His expertise, flexibility, patience, and dedication are qualities that I've admired and appreciated ever since I began my project with him. Without all of his hard work in preparing my experiments and helping me explore results together, I would not be where I am today as a researcher. Thank you to Peter Weisel for all the fun laughs that we have in the lab and for your dedication in the analysis portion for this project while creating beautiful figures for the poster that I would have never achieved. Thank you to Gabby Tabor for all the silly moments that we've had together and for teaching me how to make the most important liquid ever, YEA.

I would also like to thank Dr. Dare Baldwin for serving as my CHC committee representative and for the encouragement when I thought I was behind schedule. Thank you to Karl Reasoner and the Hui Undergraduate Research Scholars Program for financial support and valuable career insights. Finally, thank you to my family and friends for their unconditional support, for being there while I rant about random things, believing in me, and making sure that I don't spend too much time on schoolwork so I can enjoy life and what UO has to offer beyond academics.

Table of Contents

List of Figures

List of Tables

Introduction

Fission yeast as a model organism

Fission yeast, scientifically known as *Schizosaccharomyces pombe*, has emerged as a valuable model organism in molecular biology research, particularly in the field of transcription. Its simple yet highly conserved genetic makeup, along with its ease of manipulation and rapid growth, makes it an ideal candidate for studying various cellular processes, including transcriptional regulation (Vyas et al., 2021; Hayles & Nurse, 2017). One of the key advantages of using fission yeast in transcriptional studies is its compact genome, which contains around 5,000 genes (Vyas et al., 2021). This streamlined genome simplifies identifying and characterizing transcription factors, promoters, and other regulatory elements involved in gene expression. Additionally, many of the genes and regulatory pathways found in fission yeast are conserved across eukaryotic organisms, including humans, making findings from studies in this organism highly relevant to understanding transcriptional regulation in higher eukaryotes (Vyas et al., 2021; Hayles & Nurse, 2017).

Moreover, fission yeast offers powerful genetic tools for manipulating gene expression and studying transcriptional mechanisms. Techniques such as gene deletion, overexpression, and site-directed mutagenesis can be easily performed in fission yeast, allowing researchers to investigate the roles of specific genes and regulatory elements in transcription (Vyas et al., 2021). Furthermore, the availability of genome-wide techniques such as chromatin immunoprecipitation followed by sequencing (ChIP-seq) and RNA sequencing (RNA-seq) enables comprehensive analyses of transcription factor binding sites, histone modifications, and gene expression profiles on a global scale (Vyas et al., 2021). Another advantage of using fission

yeast is its well-characterized cell cycle, which is tightly regulated at the transcriptional level. The transition between different cell-cycle phases involves precise temporal control of gene expression, with many key regulators being transcriptionally regulated (Hayles & Nurse, 2017). Studying the transcriptional dynamics during the cell cycle in fission yeast provides valuable insights into the mechanisms underlying cell cycle progression and coordination with other cellular processes.

Central dogma and transcription factors

The fundamental principle guiding biological processes, known as the central dogma, delineates the unidirectional flow of genetic information: DNA to RNA to proteins. This flow is orchestrated by key processes including DNA replication, transcription, and translation. DNA replication safeguards genetic materials and ensures every cell maintains a complete genome. Transcription, following replication, involves the synthesis of RNA strands complementary to specific DNA sequences. Translation decodes RNA to produce polypeptides that fold into functional proteins (Cobb, 2017).

Within these processes, regulatory factors exert control over genetic flow. In transcription, transcription factors play pivotal roles in modulating gene expression by influencing the transcription of genes from DNA to RNA. Transcription factors initiate transcription by binding to specific DNA sequences, thereby promoting transcription. By binding to sequences upstream of the promoter, transcription factors govern the activity of RNA polymerases, which are enzymes responsible for transcribing DNA into RNA (Lescure et al., 1994). Different RNA polymerases transcribe various types of RNA, yielding diverse products. For example, RNA polymerase I (Pol I) transcribes rRNA, Pol II transcribes mRNA, miRNA,

snRNA, and snoRNA, while Pol III transcribes tRNA and 5S rRNA (Carter & Drouin, 2009). This intricate regulatory mechanism finely tunes gene expression, ensuring the unique and dynamic profiles required for different cell types and developmental stages (Lescure et al., 1994). Among the crucial transcription factors involved in this regulatory network is the TATA-box binding protein (TBP), which plays a pivotal role in coordinating transcriptional processes.

TATA-box binding protein (TBP)

TBP function has been well known for a general transcription factor that can regulate all three types of RNA polymerases, referred to as Pol I, Pol II, and Pol III (Carter & Drouin, 2009; Lee & Young, 1998). Together, this complex can recognize the promoter region, allowing RNA polymerases to attach at the correct location to begin transcription. Specifically, TBP can bind to the TATA box through an induced-fit mechanism of protein-DNA recognition, where TBP undergoes a conformational change of its bound DNA and induces DNA bending (Kuddus & Schmidt, 1993; Hernandez 1993; Anandapadamanaban et al., 2013). Previously, studies supported that transcription activation is promoter-specific and is sensitive to mutations on the DNA-binding surface of TBP rather than a fortuitous activation domain on TBP, suggesting that the recruitment of TBP to the promoter can be a rate-limiting step for transcription in vivo (Chatterjee & Struhl, 1995). Consistently, findings have shown that RNA polymerase II transcription can be mediated through mammalian complexes independent of TBP in vitro, pointing to the possibility that TBP may not have a universal role in transcription and may have other specific and distinct functions in vivo (Davidson, 2003).

TBP N-terminus

Remarkably, TBP exhibits conservation across eukaryotes and certain archaebacteria species, underscoring its significance across diverse organisms, including humans. Comparative analysis of TBP sequences across organisms has unveiled a highly conserved carboxy-terminal domain, contrasting with the non-conserved nature of the amino-terminal domain (Hernandez, 1993). Although the amino-terminal domain displays a variable sequence and length among organisms, it plays crucial roles in regulating the TBP-DNA complex (Kuddus & Schmidt, 1993; Hobbs et al., 2002; Lescure et al., 1994) Moreover, the N-terminus is characterized by its flexibility, potentially influencing the conformation of DNA and its interactions with other molecules (Kuddus & Schmidt, 1993; Kim et al., 1995; Seipel et al., 1993). Nonetheless, the precise functions and mechanisms of the N-terminal domain remain elusive.

Deletion studies targeting the entire N-terminus of TBP have demonstrated diminished transcription rates, indicating its role in shaping the stability and conformation of the TBP-DNA complex. This conformational alteration facilitates DNA bending, thereby modulating its binding activity, as observed in yeast models (Kuddus & Schmidt, 1993). Similarly, investigations involving modified mammalian TBP proteins have shown that mutants lacking the N-terminal domain exhibit midgestational lethality attributed to placental defects, suggesting a potential involvement in transcriptional regulation conducive to maternal immunotolerance during pregnancy (Hobbs et al., 2002). Studies on human TBP further elucidated that specific regions within the N-terminal domain may facilitate essential protein-protein interactions necessary for assembling functional preinitiation complexes on TATA-containing promoters (Lescure et al., 1994). Consistent with previous findings, research indicates that TBP serves as an auxiliary activation domain, bolstering the activity of other factors bound to promoters in humans (Xing et

al., 2008). These insights underscore the multifaceted roles of the TBP N-terminus in orchestrating transcriptional processes across various organisms.

3D genome organization

The burgeoning field of 3D genome has sparked considerable interest within the scientific community in recent years. Advances in high-throughput sequencing technology have unveiled that linear 1D DNA sequences are intricately organized into 3D chromatin structures, referred to as 3D genome organization (Szabo et al., 2019). This organization is vital for accommodating all the DNA within the nucleus of each cell. However, the precise mechanisms and factors governing this compaction process remain elusive. Evidence over the years has supported the existence of multiple levels of organizational structures, ranging from the DNA double helix to nucleosomes, chromatin loops, topologically associated domains, A and B compartments, and ultimately, chromosome territories, spanning from smaller to larger scales, respectively (Jerkovic & Cavalli, 2021). Within these topologically associated domains, emerging data suggests the presence of smaller interacting domains comprising only a few genes (Hsieh et al., 2016), in which are termed gene domains in this thesis.

At each organizational level, various proteins, complexes, and transcription factors play pivotal roles in modulating the compaction of chromatin. Several protein complexes containing structural maintenance of chromosome (SMC) factors have been identified, forming ring-shaped structures that serve as chromatin linkers. Notably, the cohesin protein complex, in conjunction with the CCCTF-binding factor (CTCF), is essential for both the formation and delineation of chromatin loops (Li et al., 2020). Another key complex, condensin, alongside cohesin, plays crucial roles in mitotic chromosome assembly and maintaining the structure of sister chromatids (Paul et al., 2018). Furthermore, transcription factors have been found to form liquid-liquid

condensates through a process called phase separation, indicative of cells self-organizing into membrane-less compartments (Boija et al., 2018). This suggests that transcription factors play a role in 3D genome organization. Notably, the flexible N-terminus of TBP, capable of regulating transcription across all three types of RNA polymerases, holds significant potential in this regard. This is reinforced by the observation that TBP binding sites coincide with gene domain boundaries, implicating TBP in the formation of gene domains, especially in eukaryotic yeast models (Figure 1).

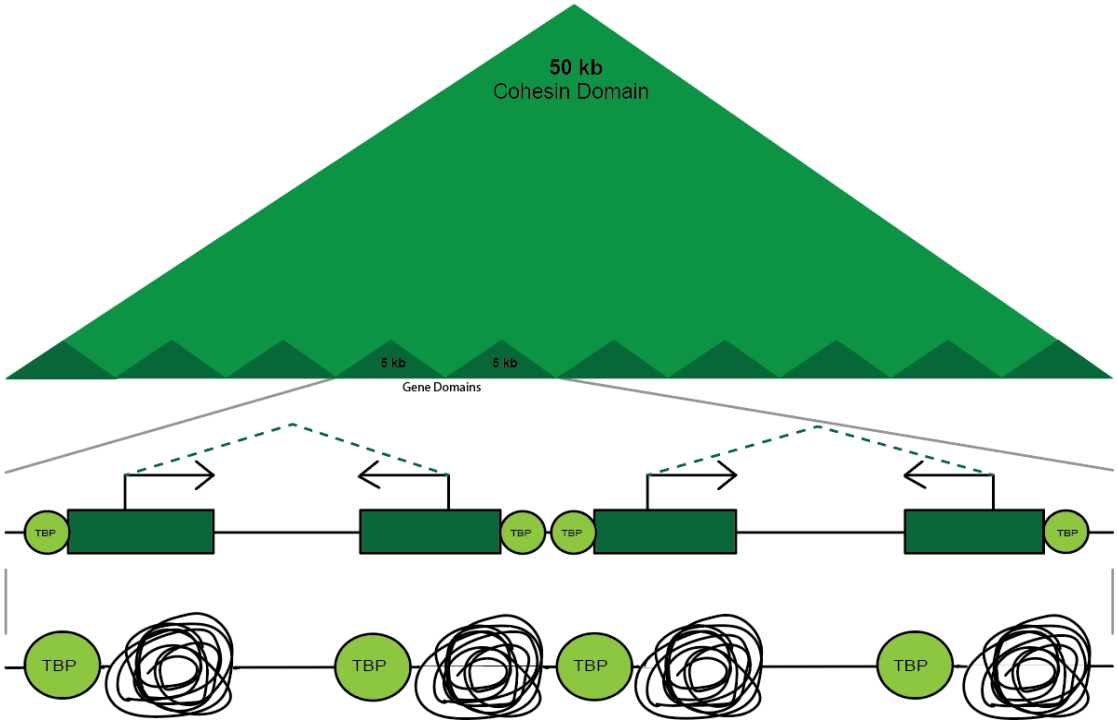

Figure 1. Model of Gene Domains. Gene domains are small chromatin domains that contain only a few genes found within topological domains such as the cohesin domain. TBP is found at gene domain boundaries, implicating TBP in the formation of gene domain boundaries.

TBP and condensin

Expanding upon prior investigations into condensin-mediated 3D genome organization, it has been elucidated that Pol III genes, such as tRNA and 5S rRNA genes, exhibit a dispersed distribution across chromosomes while also forming associations with centromeres (Iwasaki et al., 2015). Recent studies have shed light on the pivotal role played by the interaction between the kleisin subunit of condensin and the transcription factor TBP in orchestrating this intricate process of genome organization in the fission yeast model. Through meticulous experimentation, it was unveiled that the kleisin subunit is recruited to Pol III and Pol II genes via its direct interaction with TBP, an essential factor in transcription initiation (Iwasaki et al., 2015). To rigorously examine the functional significance of this interaction, a targeted mutation in the *cnd2* condensin gene was employed, effectively disrupting the binding interface between Cnd2 and TBP. Consequently, the recruitment of condensin across the genome was profoundly compromised, resulting in pronounced defects in chromosomal segregation and culminating in cellular lethality (Iwasaki et al., 2015). This compelling evidence underscores the indispensable nature of the interplay between TBP and condensin in facilitating the intricate three-dimensional organization of chromosomes, which in turn ensures the faithful segregation of actively transcribed genes. Furthermore, the implications of these findings extend beyond mere cellular processes, as aberrant chromosome segregation patterns have been intimately linked to the onset and progression of various diseases, notably cancer (Potapova & Gorbsky, 2017). Similarly, cellular lethality arising from disruptions in genome organization holds relevance to a spectrum of pathological conditions, including developmental disorders and neurological diseases. Thus, the elucidation of the molecular mechanisms governing 3D chromosome organization, particularly in the context of TBP-condensin interactions, not only provides invaluable insights

into potential strategies for disease prevention but also offers a deeper understanding of the pathogenic mechanisms underlying a myriad of disorders stemming from perturbations in genome architecture.

TBP-N terminus in gene regulation and 3D genome organization

Using fission yeast as a model system, this thesis aims to determine how the TBP-N terminal region affects the formation of gene domains under stress conditions via the process of phase separation. By creating a manipulated TBP N-terminus by removing various lengths of the N-terminus, transcription and cell maintenance regulation processes may be revealed through the perspective of 3D genome organization. This study supported the idea that several stress conditions, such as heat stress, affect the phenotypes of mutant cells. Using a Pk-epitope tag, immunofluorescence and DAPI microscopy revealed disruptions in TBP localization in mutant cells. Finally, analyses on high-throughput sequencing data, such as ChIP-seq, RNA-seq, and Hi-C, provided further insight into how TBP and its mutant strains affect TBP binding, gene expression, and gene domain formation. In summary, the TBP N-terminus has important roles in proper stress responses in fission yeast cells and is critical for maintaining faithful segregation of transcribed genes and proper 3D genome structure.

Methods

The present study aims to examine the function and mechanism of TBP N-terminus in the formation of gene domains via phase separation under stress conditions. For this research, we first created TBP N-terminal mutants by cutting off 25 or 50 amino acids of the N-terminus to examine how the lack of N-terminal regions affects the way that TBP functions in the organization of DNA. The N-terminal mutants are validated through PCR and gel electrophoresis, procedures that can amplify regions of DNA and visualize the length of samples. In successful mutants, the bands observed on the gel were expected to be shorter than wild-type. Mutants were also duplicated and tagged with a Pk-epitope for visualization experiments later. A series of growth assay experiments were subsequently performed with the created strains. These experiments included spot tests and doubling-time experiments, which would show the phenotypes of mutant cells. This was performed under different stress conditions to see what conditions resulted in high sensitivity from the mutants. Immunofluorescence and DAPI microscopy were performed after identifying stress conditions from growth assay experiments to observe nuclear TBP localization and how it may be disrupted in mutants. Finally, an analysis of ChIP-seq, RNA-seq, and Hi-C data was performed to compare how TBP affects localization, gene expression, and gene domains, which gave insights into how the TBP N-terminus is necessary for proper stress response.

Fission yeast strains

The fission yeast *Schizosaccharomyces pombe* strains used in this study are listed below:

Strain ID	Genotype
SPSTn245	*h^{+N} ade6-M210 leu1-32 ura4-DS/E*
SPSTn807	*h^{+N} ade6-M210 leu1-32 ura4-DS/E 4Pk-tbp1*
SPSTn817	*h^{+N} ade6-M210 leu1-32 ura4-DS/E tbp1-N25Δ*
SPSTn850	*h^{+N} ade6-M210 leu1-32 ura4-DS/E tbp1-N50Δ*

SPSTn857 *h+N ade6-M210 leu1-32 ura4-DS/E 4Pk-tbp1(N50Δ)*
SPSTn1021 *h+N ade6-M210 leu1-32 ura4-DS/E tbp1-4Pk-kanMX6*
SPSTn1024 *h+N ade6-M210 leu1-32 ura4-DS/E tbp1(N25Δ)-4Pk-kanMX6*
SPSTn1025 *h+N ade6-M210 leu1-32 ura4-DS/E tbp1(N50Δ)-4Pk-kanMX6*

Culture and media plate conditions

Cells were grown on yeast extract adenine (YEA) plates, a complete medium supplemented with adenine, in a 30°C incubator. YEA plates consist of 30 g/L D-glucose, 5 g/L yeast-extract, 100 mg/L adenine, and 20 g/L agar, where the solution is adjusted to the pH of 5.5 with hydrochloric acid and autoclaved at 121°C for 15 minutes before setting in the plates. For the spot test experiments, the following medium plates were prepared: YEA containing 5 mM hydroxyurea (HU), 1 mM hydrogen peroxide (H_2O_2), 5 mM camptothecin (CPT), or thiabendazole (TBZ) (5, 10, or 15 μg/ml). For the IF experiments, 5 mM HU or varying concentrations of 1,6-Hexanediol (HD) (1.25, 2.5, 5, 6, 7, 8, 9%) solutions were added to YEA liquid cultures. All stock solutions besides HD were prepared with autoclaved water. HD solutions were prepared with YEA liquid media (described above except agar powder).

Fission yeast colony PCR

Small amounts of cells growing on a YEA plate were suspended in 10 μl of 2 mg/ml zymolyase-100T before being incubated at 37°C for 1 hour. The cell suspensions were incubated at 96°C for 5 minutes and 90 μl of water was added to each sample. After centrifugation at 10,000 rpm at room temperature for 1 minute, 0.5 μl of the lysate was used for PCR reaction as follows. In an ice bucket, the PCR mix was made using 0.05 μl of primer, 2.5 μl of Onetaq DNA polymerase, and 1.95 μl of water per sample, in which the primers used included STn521 (CGTCGAGACTGCTGAAG) and STn550 (AGGCACGACTTACTCTAAG). The PCR mix (4.5 μl per sample) was transferred into PCR tubes, and 0.5 μl of the lysate was added to their

respective PCR tubes. The samples were placed in the PCR machine under three stages. In stage one, the samples endured initial denaturation for 30 seconds at 94°C. In stage two, the samples were denatured for 15 seconds at 94°C, the primers were annealed to specific genomic regions for 15 seconds at 55°C, and the DNA was extended for 1 minute at 68°C. Stage two was repeated 30 times before reaching stage three. In stage three, the samples endured their final extension for 5 minutes at 68°C before being stored at 4°C until the samples were taken out. Each sample (2 µl) was used to run gel electrophoresis at 100V for 25 minutes before DNA staining with ethidium bromide, followed by UV imaging.

Doubling time

Cultures were made the day prior to the experiment to allow cells to reach the mid-log phase, in which the cells were cultured overnight in 5 ml of YEA liquid media at 30°C with shaking. All samples were diluted to optical density at 595 nm (OD595) 0.05 on the Ultrospec 2100 pro spectrophotometer and were incubated for 1 hour at 30°C with shaking after dilution. The conditions using the spectrophotometer maintained the same throughout the experiment. The OD595 was collected after incubation and counted as hour 0. The samples were incubated at 30°C with shaking and the OD595 was collected every 2 hours after hour 0. The average doubling time and standard deviation were calculated and plotted using Excel.

Spot tests

Cultures were prepared after mixing a period-sized amount of colony and 1 mL of YEA, in which the cultures were diluted to OD595 0.5. Using a 96-well plate, 100 µl of each sample culture was transferred into the 1st column of the plate. Water (80 µl) was placed in the next 5 wells per sample. A ⅕ serial dilution was then performed by transferring 20 µl along each

column, starting from the 1st column containing the OD 0.5 cultures. Samples from all wells (5 µl) were spotted on YEA plates with and without HU, H_2O_2, CPT, or TBZ (see "Culture Conditions" above). The plates were incubated at 30°C, while some plates were placed at 26°C or 37°C to test for temperature sensitivity. Images of the plates were scanned using the Epson Perfection V700 photo scanner between 2-4 days after incubation.

DAPI (4′,6-diamidino-2-phenylindole) microscopy

Cultures were prepared after mixing mutant colonies with 5 mL of YEA before incubating overnight at 30°C or 37°C with shaking. For the short-term heat stress condition, cultures were incubated at 30°C overnight and incubated additionally at 37°C for 4 hours. After incubation, the cultures were adjusted to OD 0.45, and 900 µl of culture per sample was transported into iced centrifuge tubes filled with 100 µl formaldehyde. The tube containing the culture and formaldehyde was vortexed for at least 10 seconds before being chilled in the ice bath for 30 minutes. The samples were centrifuged at 4°C for 3 minutes at 5,000 rpm, and the supernatant was discarded for each sample to leave behind the pellet. 500 µl of PBS was mixed into each sample. The centrifugation, discard of supernatant, and addition of PBS were repeated 2 additional times. During the last round of centrifugation, the supernatant was discarded, though no additional PBS was added. The pellets were suspended in 20 µl PBS and stored at 20°C. The cells were mounted on a coverslip with a mounting medium containing 1 µg/mL 4′,6-diamidino-2-phenylindole (DAPI) dilactate and 100 µg/mL p-phenylenediamine and subjected to imaging with the DeltaVision microscope.

Immunofluorescence (IF) microscopy

Cells were cultured in 9 mL YEA to mid-log phase at 30°C with shaking overnight. For experiments testing HU sensitivity, HU was added to each sample (final 5 mM HU in each culture) before culturing overnight at 30°C. For the HD-treated experiments, 9 mL of varying concentrations of HD were added to each sample (final concentrations varying from 1.25~9%) and incubated at room temperature for 5 minutes after the overnight incubation at 30°C. One mL of 30% paraformaldehyde was added to each sample before being incubated for 60 minutes at 30°C with shaking. For the HD-treated experiments, 2 mL (rather than 1 mL) of 30% paraformaldehyde was added to maintain the correct ratio. The samples were centrifuged at 2,000 rpm for 3 minutes, and the supernatant was discarded. Samples were suspended in 500 µl PEM (100 mM PIPES, 1 mM EGTA, 1 mM $MgSO_4$), and the suspensions were transferred to 1.5 mL centrifuge tubes. The samples were centrifuged at 3,000 rpm at room temperature for 3 minutes before discarding the supernatant. The cells were washed once with 500 µl PEM, and once with 500 µl PEMS (100 mM PIPES, 1 mM EGTA, 1 mM $MgSO_4$, 1 M sorbitol) before being suspended in 490 µl PEMS. Ten µl of 10 mg/mL zymolyase 100T was added to each sample, and the samples were incubated at 37°C for at least 20 minutes with rotation. After 20 minutes, cell wall digestion was evaluated under a microscope to check if cell walls of at least 90% of the cells were digested. If the digestion frequencies were less than 90%, the samples were incubated at 37°C for additional time until the digestion frequencies reached 90%. The cells were washed three times with 500 µl PEMS, followed by suspending the cells in 450 µl of PEMS. Fifty µl of 10% Triton X-100 was added to each sample, and the samples were incubated for 2 minutes at room temperature. The cells were washed twice with 500 µl of PEMS and twice with PEM before being suspended in 500 µl of PEMBAL (100 mM PIPES, 1 mM EGTA, 1 mM

MgSO4, 1% BSA, 0.1% sodium azide, 0.1 M L-lysine) and incubated at room temperature for 60 minutes with rotation. The cells were centrifuged at 3,000 rpm at room temperature for 3 minutes, and the supernatant was discarded. The cells were suspended in 100 µl of the primary antibody solution (see below) and incubated at room temperature overnight with rotation. The cells were washed three times using 500 µl PEMBAL before suspending the cells in 250 µl PEMBAL and incubated at room temperature for 30 minutes with rotation. The secondary antibody solution (250 µl; see below) was added to each sample and the sample was incubated at room temperature for more than 2 hours with rotation in the dark. The cells were washed 3 times with 500 µl PEMBAL at 15-minute intervals in the dark before suspending the cells in 100 µl PEMBAL. The suspended cells were stored at 4°C until imaging. For imaging, 1 µl of cell suspension was spread on a poly-L-lysine coverslip, and the coverslip with mounted with 3 µl of mounting medium (50% glycerol, 1 µg/ml DAPI, 0.1 mg/ml paraphenylene diamine) before using the DeltaVision microscope.

Antibodies used for IF experiments

The primary antibody used for IF experiments to visualize Pk-tagged TBP proteins was the Pk antibody, while the secondary antibody was anti-mouse IgG Cy3. Alternatively, anti-Cnd2 antibody (rabbit IgG) and TAT-1 antibody (mouse IgG) were used as primary antibodies to detect condensin and tubulin, respectively. For this experiment, anti-rabbit IgG Alexa488 and anti-mouse IgG Cy3 were used as secondary antibodies. All antibody solutions were diluted with PEMBAL at a 1:1000 ratio.

ImageJ analysis

Images taken from DeltaVision stained for DAPI were analyzed using the ImageJ software. The threshold was adjusted to best fit the size of the nucleus of each strain, and the generated data regarding the area of the nucleus was recorded in Excel for each image. All cells that did not show a full nucleus, such as those where the nucleus is at the image border were excluded. All cells with poor threshold-fitting, i.e., the threshold didn't cover the entire nucleus or cover more than the nucleus, were also excluded. The mean area and its standard deviation of nuclei for each strain were then calculated by Excel.

Statistical Analysis (Doubling Time and ImageJ Analysis)

All statistical analyses were conducted using Excel. For the doubling time experiments, unpaired two-tailed t-tests with an alpha value of 0.05 were used to compare mutant strains with the WT strain. For ImageJ analysis, an ANOVA test was used in addition to unpaired two-tailed t-tests with an adjusted Bonferroni alpha value of 0.0167 to analyze differences between strains. Significant differences with $p<0.05$ were indicated by *. Furthermore, ** and *** indicate significant differences with $p<0.01$ and $p<0.001$, respectively.

RNA-seq analysis criteria

RNA-seq results of the wild-type, TBP-N25Δ, and TBP-N50Δ (performed by Dr. Tashiro; unpublished) were visually analyzed on the IGV browser. All genes that had higher signal intensities in TBP-N50 compared to TBP-WT were recorded, as well as genes that had higher signal intensities in TBP-N25 compared to TBP-WT. The functions of the recorded genes were searched through PomBase (fission yeast community website; https://www.pombase.org).

ChIP-seq analysis criteria

ChIP-seq results of the TBP-Pk, TBP(N25Δ)-Pk, and TBP(N50Δ)-Pk (performed by Dr. Tashiro, unpublished) were visually analyzed on the IGV browser. All genes that had a 2-fold or higher difference between strains were recorded, whether that difference is higher or lower compared to WT. The functions of the recorded genes were searched through PomBase and used to compare with RNA-seq results.

Hi-C analysis

Hi-C results of the wild-type, TBP-N25Δ, and TBP-N50Δ (performed by Dr. Tashiro; unpublished) were visually analyzed on the Juicebox browser. Genes noted from RNA-seq and ChIP-seq were identified in Hi-C data to observe levels of interaction within the chromosome.

Results

TBP-NΔ mutants were generated and confirmed through PCR

The TBP-NΔ mutants (NΔ25 and NΔ50) were generated through the deletion of 25 and 50 amino acids from the N-terminal end of TBP by Dr. Tashiro. The wild-type (WT) and TBP-NΔ strains were grown at 30°C and stored on YEA plates. This temperature was chosen as wild-type fission yeast cells grow ideally at 30°C (Peterson & Russell, 2016). Using the primers 521 and 550, I verified the genomic deletion through PCR amplification (Fig. 2A). The PCR-amplified DNA fragments were visualized using gel electrophoresis (Fig. 2B). PCR analysis confirmed the generation of both WT TBP sequence and mutants with 25 (NΔ25) and 50 (NΔ50) amino acids removed from the N terminus. The presence of distinct PCR bands corresponding to the WT and mutant sequences indicated the successful generation of the desired mutants, with WT bands being 0.7 kb in length and shorter bands for NΔ25 and NΔ50. These results validated the efficacy of the designed primers in inducing specific deletions in the TBP-N terminus.

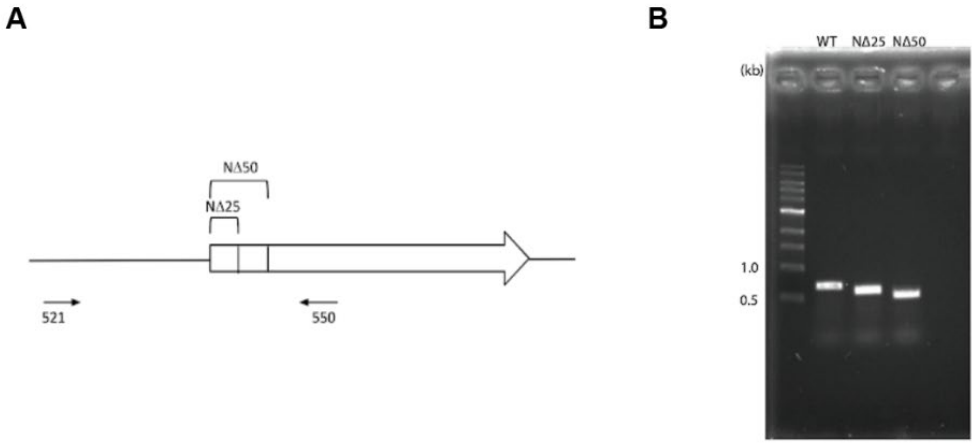

Figure 2. Construction of TBP-NΔ mutants. (A) Schematic representation illustrating TBP-NΔ25 and Δ50 mutations and detection of those deletions by PCR using primers 521 and 550. (B) Gel electrophoresis depicting PCR results of the wild-type TBP sequence and mutants with 25 (NΔ25) and 50 (NΔ50) amino acids removed from the N terminus.

TBP-NΔ mutants grow slowly and exhibit sensitivity to certain culturing conditions

To examine the phenotypes of the TBP-WT and NΔ (NΔ25 and NΔ50) strains, I performed doubling time experiments with the TBP-WT and NΔ strains and analyzed the impact of TBP-NΔ mutations on the average doubling time of the strains, both with and without Pk epitope tags at the C-terminus of TBP (Fig. 3). The TBP-NΔ mutants generally exhibited a slower doubling time compared to WT strain with a doubling time of 2.56 ± 0.636 hours, such that the TBP-NΔ50 strain displayed the most pronounced delay with a doubling time of 5.41 ± 0.603 hours ($p=0.0006$). The TBP-NΔ25 strain exhibited a slightly slower doubling time compared to WT, with a doubling time of 3.02 ± 0.233 hours ($p=0.02$). Interestingly, the presence of Pk tags tended to decrease doubling time in TBP-NΔ mutant strains. Specifically, the TBP-NΔ50-Pk strains decreased the doubling time to 3.09 ± 0.061 hours in the presence of Pk tags ($p=0.005$). Similarly, the TBP-NΔ25-Pk strain decreased the doubling time to 2.81 ± 0.344 hours, though it was not significantly different from WT strains. Statistical analysis revealed significant differences between the WT strain compared with TBP-NΔ25, NΔ50, and NΔ50-Pk strains (Fig. 3). These data indicated that the inclusion of Pk tags, notably positioned at the C-terminus of TBP, appeared to impact the growth dynamics, specifically the doubling time of TBP-N Δ strains, suggesting a potential role in regulating the function of TBP with respect to its length.

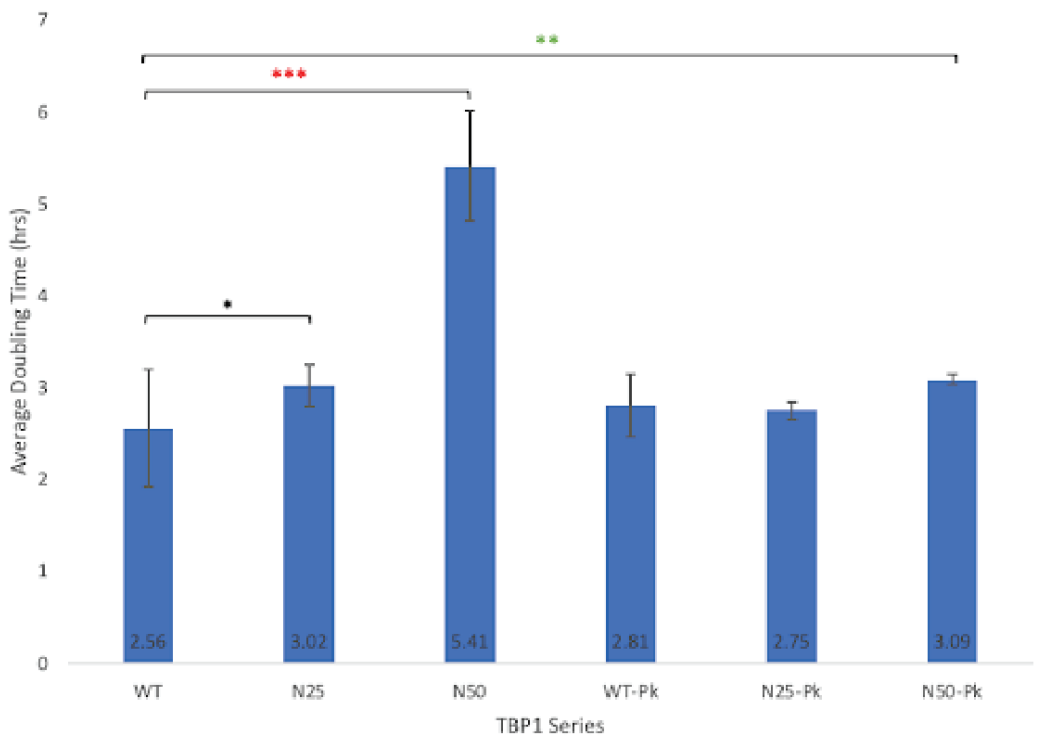

Figure 3. The average doubling time of the wild-type (WT) and NΔ TBP strains. The TBP-WT and ΔN carrying Pk-epitope at their C-termini tagged strains. Data is presented as mean +/- standard deviation (error bar). Significant differences were found between the TBP-WT and NΔ25 strains (p=0.02)*, WT and NΔ50 (p=0.0006)***, and WT and N50-Pk (p=0.005)**.

To further investigate the slower growth exhibited by the TBP-NΔ strains, I performed spot tests on the TBP-WT and NΔ strains under multiple culturing and plate conditions (Fig. 4). For control, fission yeast spots were grown on YEA plates at 30°C. Under this condition, WT cells showed a normal growth as expected, while TBP-NΔ50 cells exhibited growth reduction, confirming the results found in the doubling time experiments. In contrast to TBP-NΔ50 cells, the TBP-NΔ25 mutant displayed growth patterns similar to the WT strain across most conditions tested. Similarly, the presence of a Pk epitope tag rescued the growth of all strains. The TBP-WT and TBP-NΔ strains with Pk tags exhibited more growth overall compared to their non-tagged counterparts (Fig 4A). Since TBP-NΔ25 cells had similar growth patterns compared to WT, I

focused on observing sensitivity differences in NΔ50 mutants. Specifically, the TBP-NΔ50 mutant showed higher sensitivity towards temperature, especially when cells were cultured in 37°C. In these experiments, high sensitivity was defined as severe reductions in growth compared to strains cultured at 30°C. Additionally, the TBP-NΔ50 mutant showed sensitivity to the exposure to 5mM hydroxyurea (HU), a small molecule drug that inhibits the cell cycle during the S phase (Xu et al., 2016) (Fig 4A). Surprisingly, the TBP-NΔ50 mutant did not show enhanced sensitivity towards other chemicals, such as potassium chloride (KCl) (Alao et al., 2015), hydrogen peroxide (H_2O_2) (Pekmez et al., 2008), and camptothecin (CPT) (Collura et al., 2005), conferring osmotic, oxidative and DNA-damage stresses, respectively (Fig. 4B). The TBP NΔ50 mutant displayed a minor or no sensitivity compared to WT across all tiabendazole (TBZ) conditions (Fig. 4C). Moreover, the TBP WT and NΔ strains carrying the Pk epitope tag showed comparative growth after different doses of UV irradiation (Fig. 4D). Since the spot test experiments supported high sensitivity of the TBP-NΔ strains against the elevated temperature (37°C) and HU, these culturing conditions will be utilized and focused on further experiments described later. Overall, these efforts provide valuable insights into the physiological effects of the TBP-NΔ mutations and their implications in cellular fitness under diverse environmental stresses.

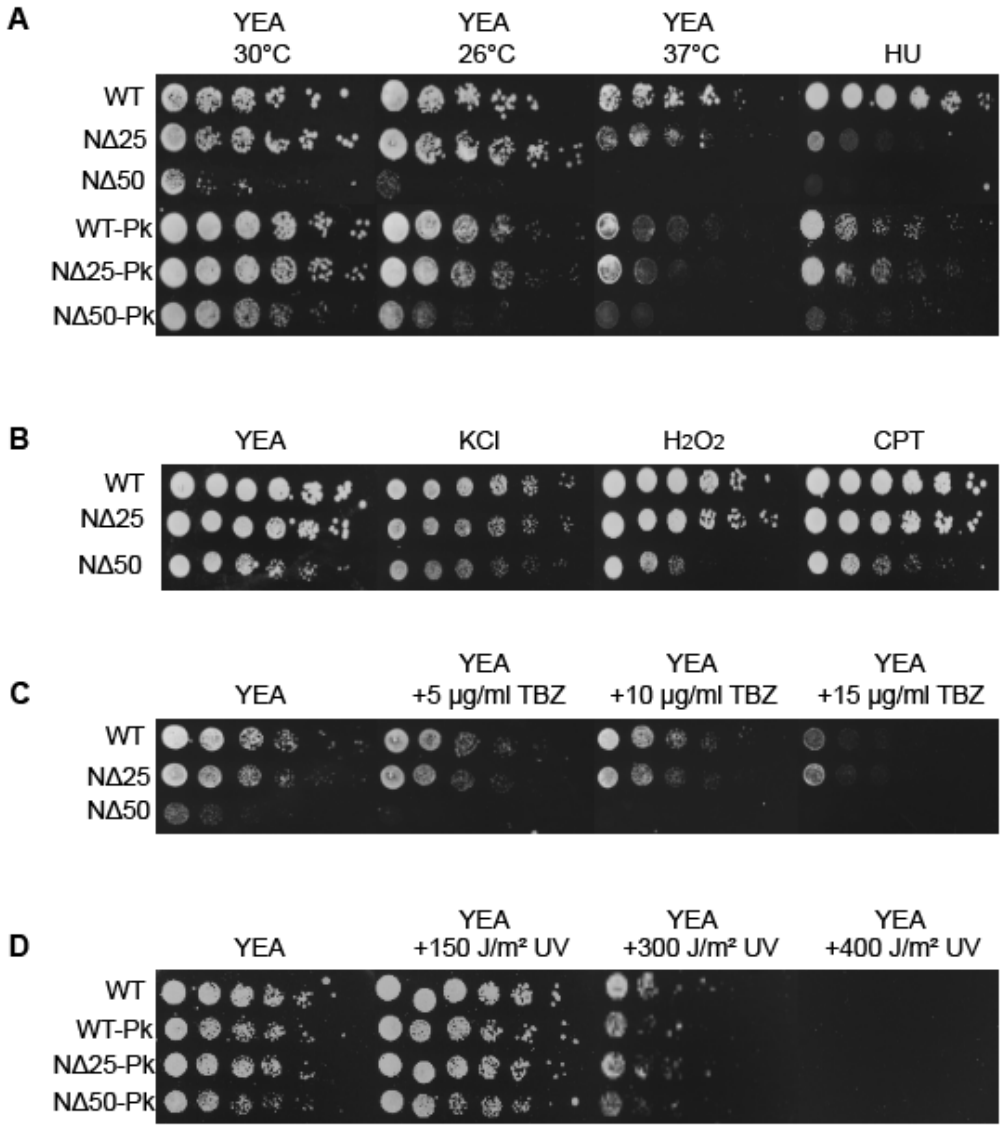

Figure 4. Spot tests of the TBP WT and NΔ strains under different culturing conditions. The TBP-NΔ50 mutant showed severe reductions in growth overall, while the TBP-NΔ25 mutant showed similar growth patterns as the WT strain. (A) Spot tests of the TBP WT and NΔ strains with and without the Pk epitope against the indicated culturing conditions. (B) Spot tests of the TBP WT and ΔN strains against potassium chloride (KCl), hydrogen peroxide (H2O2), and camptothecin (CPT). (C) Spot test of the TBP- WT and ΔN strains against tiabendazole (TBZ). (D) Spot test of the TBP-WT and ΔN strains with and without the Pk epitope against varying doses of UV irradiation

TBP-NΔ50 strain carrying a Pk epitope tag at the C-terminus resembles more closely to the TBP-NΔ50 strain

In both growth assay experiments, the presence of a Pk epitope tag significantly increased the growth of TBP-NΔ50 mutant strain under all conditions. However, the impact of incorporating a Pk epitope tag based on its position, i.e. N-terminal or C-terminal ends, remained unclear. To explore the effects of the Pk tag position on the growth of the NΔ50 strains, I performed spot tests under culturing conditions in which the TBP-Δ50 strain showed sensitivity (Fig. 5A). After several days of culturing, spot test analysis revealed the TBP-NΔ strain with the Pk epitope tag at the N-terminal end, denoted as Pk-NΔ50, exhibited markedly enhanced growth compared to untagged NΔ50 strains. This enhancement was conspicuous as it brought the growth profile of Pk-NΔ50 closer to that of the WT strain. Conversely, the TBP-Δ50 strain with the Pk tag at the C-terminus, denoted as NΔ50-Pk, also displayed increased growth relative to the NΔ50 strain without the Pk tag. However, unlike the Pk-NΔ50 strains, the growth of the TBP-NΔ50-Pk strain more closely resembled that of the NΔ50 strain (Fig. 5A).

To further elucidate the growth dynamics influenced by the appended position of the Pk epitope tag, I measured the average doubling time of the strains carrying TBP-WT, ΔN50, Pk-Δ50, or Δ50-Pk (Fig. 5B). Consistent with previous findings, the NΔ50 strain exhibited a slower doubling time of 4.896 ± 0.447 hours compared to the WT strain with a doubling time of 2.56 ± 0.64 hours. However, the incorporation of the Pk tag generally resulted in a reduction in doubling time when compared to the NΔ50 strains. Notably, the Pk-NΔ50 strain displayed a significantly shorter doubling time of 2.753 ± 0.077 hours compared to NΔ50-Pk with a doubling time of 3.09 ± 0.061 hours. Statistical analysis revealed significant differences in doubling time between the TBP-WT and the NΔ50 strains ($p=0.0002$) and between the TBP-WT and NΔ50-Pk

strains (p=0.005). Although the presence of a Pk epitope tag at the N- or C-termini of TBP-N50 improved the growth compared to the TBP-NΔ50 strain, and thereby shortened the doubling time, a Pk tag at the C-terminal end resembled untagged NΔ50 more closely compared to Pk-NΔ50. Therefore, subsequent experiments will prioritize the use of NΔ50-Pk strains to maintain consistency with the physiological characteristics of the untagged NΔ50 strain. This choice ensures that any observed effects or phenotypic changes are more likely attributable to the TBP-NΔ deletions rather than alteration in protein behavior resulting from tag positioning.

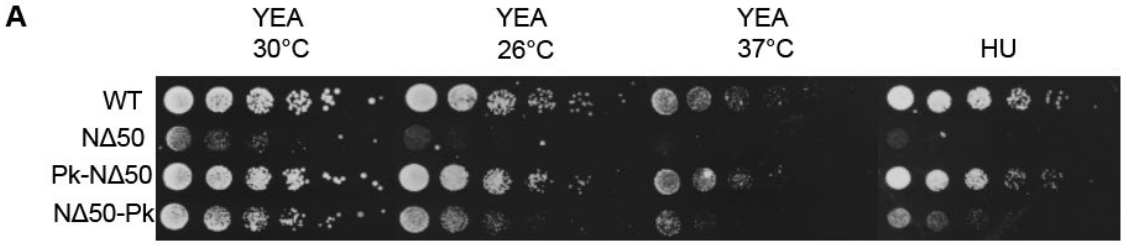

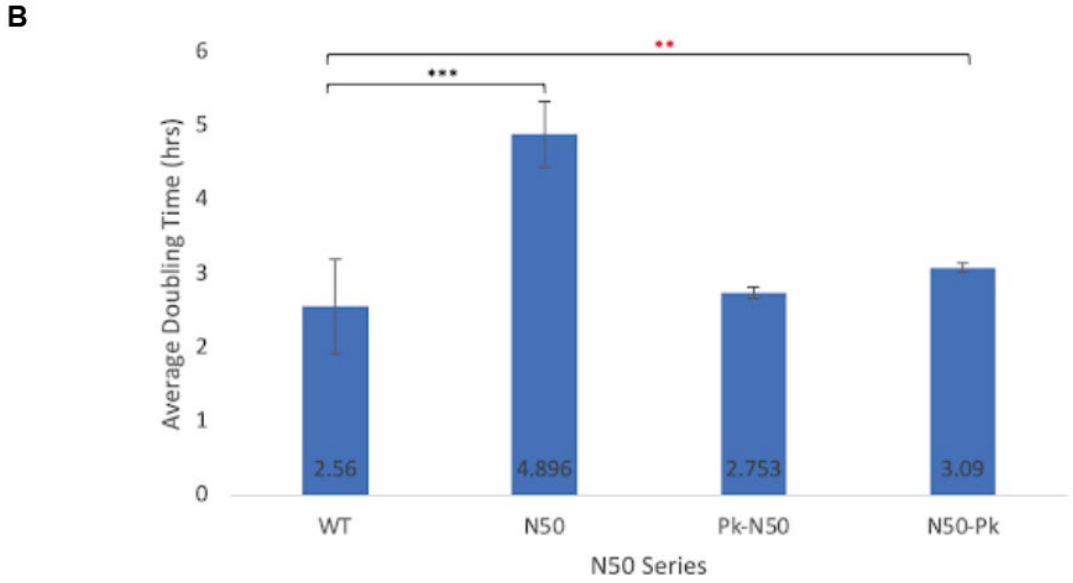

Figure 5. Pk-tag on the C-terminus of TBP-NΔ50 strain resembled more closely to NΔ50 without epitope tags. (A) Spot tests of TBP-WT, NΔ50, Pk-NΔ50 (N-terminal Pk), and NΔ50-Pk (C-terminal Pk) against different temperatures and HU. (B) The average doubling time of the indicated strains expressing TBP WT, NΔ50, Pk-NΔ50, or ΔN50-Pk tagged and non-tagged strains Significant differences were found between the TBP-WT and NΔ50 strains (p=0.0002)*** and between the TBP-WT and N50-Pk strains (p=0.005)**.

DAPI microscopy and analysis revealed alternations in nuclear morphology and size between the TBP WT and NΔ strains

Since I observed the reduction of cell growth with the TBP-NΔ strains compared to the TBP-WT strain and TBP binds to DNA, I hypothesized that the TBP-NΔ mutations would potentially display alterations in nuclear morphology. Specifically, I predicted that culturing conditions showing impaired growth characteristics of the TBP-NΔ mutant would exhibit aberrant nuclear morphologies, characterized by changes in nuclear size, shape, or organization. These alterations may reflect underlying disruptions in nuclear processes such as transcription, resulting from the perturbations induced by the TBP-NΔ mutations. To explore this possibility, I prepared TBP-WT and ΔN cells under several culturing conditions and stained them with DAPI, a fluorescent stain that binds strongly to DNA within the nucleus. Microscopic analysis of DAPI-stained cells revealed distinct nuclear morphologies at 30°C (Fig. 6A). TBP-WT cells displayed a characteristic circular nucleus shape, whereas TBP-NΔ25 cells exhibited a slightly crescent shape. Notably, TBP-NΔ50 cells showed a more pronounced crescent-shaped nucleus. Intriguingly, TBP-NΔ50-Pk cells displayed a higher proportion of cells exhibiting less crescent-shaped and more circular-shaped nuclei, resembling the TBP-WT and NΔ25 nuclei (Fig. 6A). Further investigation under heat conditions revealed dynamic changes in nuclear morphology. TBP-WT cells cultured at 30°C retained their circular nuclei, whereas those cultured at 37°C exhibited a morphology similar to TBP-NΔ50 cells at 30°C, characterized by a slimmer,

crescent-shaped nuclei (Fig. 6B). In contrast, TBP-NΔ50 cells at 37°C displayed slender nuclei, resembling a thin crescent, indicating a temperature-dependent effect on nuclear morphology.

Utilizing the ImageJ software, I quantified the nuclear area in microscopic images of the TBP-WT and NΔ mutant strains (Fig. 6C). The area was determined by using the threshold function to create outlines of nuclei. Analysis of the average nuclear size revealed significant differences among the strains (Fig. 6D). The TBP-NΔ50 strain exhibited significantly smaller nuclei of $1.395 \pm 0.330\ \mu m^2$ compared to the TBP-WT and NΔ25 strains. Conversely, the TBP-WT and NΔ25 strains displayed similar nuclear areas of $1.939 \pm 0.463\ \mu m^2$ and $2.067 \pm 0.482\ \mu m^2$, respectively. Statistical analysis confirmed significant differences between the TBP-WT and NΔ50 strains ($p=1.9 \times 10^{-9}$) and between the TBP-NΔ25 and NΔ50 strains ($p=1.12 \times 10^{-13}$). Overall, these findings provide valuable insights into the functional significance of the N-terminal region in regulating nuclear morphology and underscore the importance of further investigations to elucidate the molecular mechanisms underlying these observations.

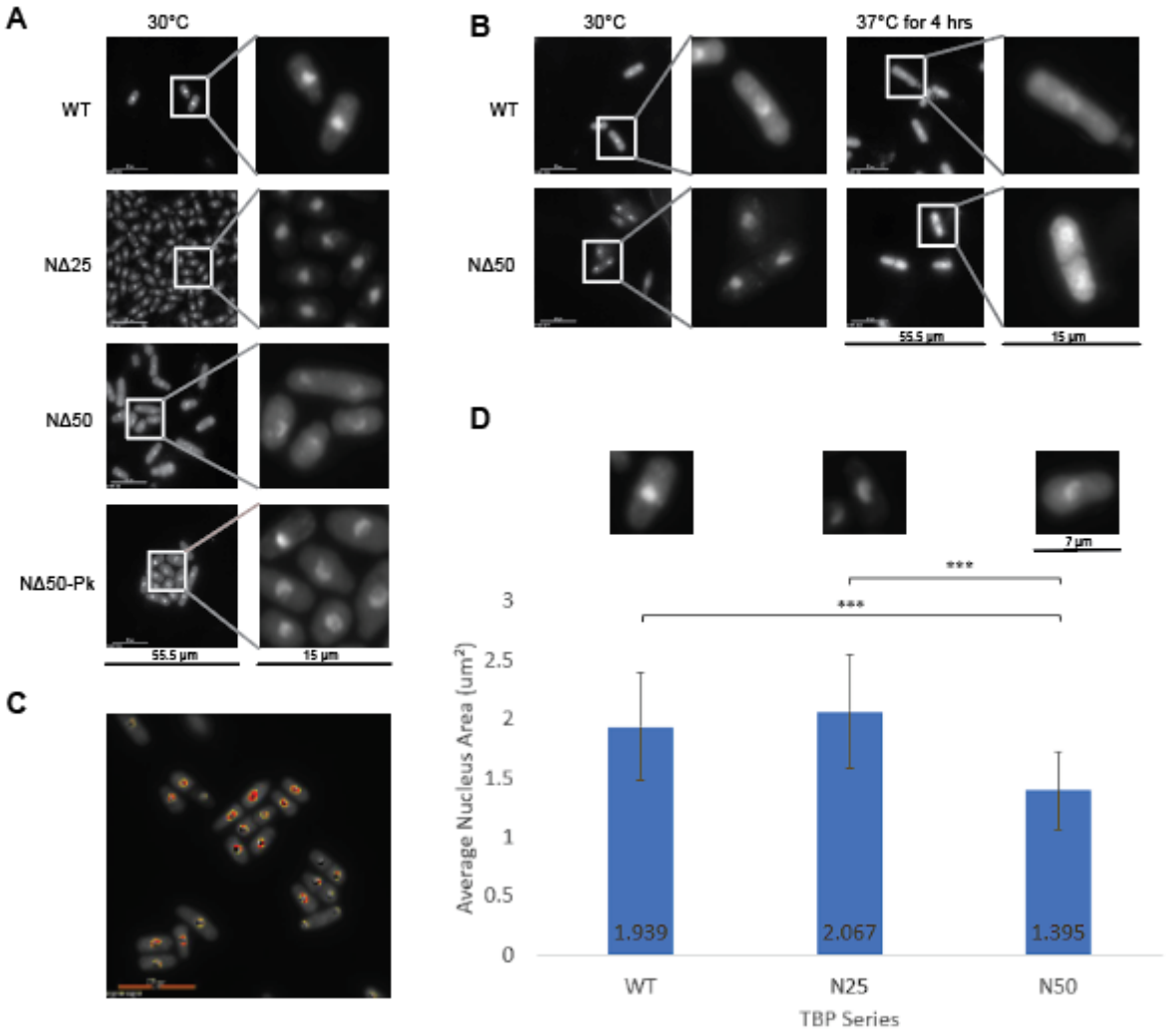

Figure 6. The TBP-NΔ mutant strains displayed alterations in nuclear morphology and size. (A) Representative images of TBP-WT, NΔ25, NΔ50, and NΔ50-Pk cells stained with DAPI. (B) DAPI-stained TBP-WT and NΔ50 cells prepared from 30 and 37°C cultures. (C) Example of nuclear area analysis using ImageJ employed in panel D. (D) Average nucleus size of the TBP-WT and NΔ strains. Data is presented as mean +/- standard deviation (error bar). Typical images from each strain are shown on top. Significant differences were found between the TBP-WT and NΔ50 strains (p=1.9E-9)***and between the TBP-NΔ25 and NΔ50 strains (p=1.12E-13)***.

IF microscopy revealed no significant differences in TBP localization between TBP-WT and NΔ strains

Using Pk-tagged strains generated previously, I examined the localization of TBP through immunofluorescent (IF) microscopy (Fig. 7). As the TBP-WT and NΔ proteins were tagged with Pk, utilizing a Pk antibody allowed for the visualization of TBP under the microscope. Regarding the localization of the TBP-WT and NΔ proteins at 30°C, TBP-WT-Pk cells exhibited a prominent Pk signal localized predominantly within the nucleus. Interestingly, visual examination did not reveal significant differences in Pk signal patterns between the TBP-WT and NΔ strains (Fig. 7A). To quantify the nuclear intensity of TBP-WT and NΔ proteins, I calculated the mean gray values, which are indicative of fluorescence intensity. The TBP-WT strains displayed a mean gray value of 20.472 ± 6.134, the TBP-NΔ25 strain displayed a mean gray value of 21.203 ± 5.404, while the TBP-NΔ50 strain displayed a mean gray value of 19.790 ± 5.762. There were no significant differences in the nuclear intensity of TBP-WT and NΔ proteins, further supporting the visual observations (Fig. 7B).

Like previous experiments, TBP-NΔ50-Pk cells were visualized under different culturing conditions, including normal growth temperature at 30°C, elevated temperature at 37°C, and exposure to 5% HU. Visual inspection did not detect significant differences in Pk signal intensity or distribution between the TBP-NΔ50 strains. However, cells cultured in the presence of 5 mM HU exhibited slightly dimmer Pk signals compared to controls (Fig. 7C). The mean gray values of TBP-NΔ50-Pk cells cultured under the three conditions were quantified (Fig. 7D). Under 37°C, TBP-NΔ50-Pk cells exhibited a mean gray value of 23.547 ± 6.259, which was similar compared to 30°C with a mean gray value of 24.025 ± 5.762. While no significant differences

were observed between 30 and 37°C, TBP-NΔ50-Pk cells exposed to 5 mM HU displayed a significantly lower mean gray value of 22.578 ± 4.404 compared to the 30°C control condition.

Previous studies have demonstrated the interaction between TBP and condensin during chromosome segregation, highlighting the importance of TBP in regulating mitotic processes. Given this established role of TBP in coordinating chromosome dynamics, it was crucial to examine the behavior of TBP-NΔ proteins during mitosis to assess whether the localization patterns of condensin and tubulin, key players in chromosome condensation and mitotic spindle formation, respectively, remain unchanged. In this experiment, DAPI (blue), tubulin TAT-1 (red), and Cnd2 condensin (green) were visualized (Fig. 7E). IF image analysis revealed no visual differences between TBP-WT and NΔ50 cells during mitosis. For both the TBP-WT and NΔ50 strains, cells in mitosis, indicated by a bright Cnd2 signal, had similar tubulin localization. Specifically, both strains presented two types of tubulin formation, one where tubulin is localized in the nucleus and another in which tubulin is localized in a line formation (Fig. 7E). Quantification analysis involved counting the number of cells with tubulin signals, in addition to what type of tubulin signal (Table 1). The results supported that in both the TBP-WT and NΔ50 strains cells had bright circular Cnd2 signals along with the presence of tubulin signals. The TBP-WT and NΔ50 strains also exhibited a similar number of cells in which tubulin is localized in the nucleus and in a line formation, both of which were typical signal localizations presented during mitosis.

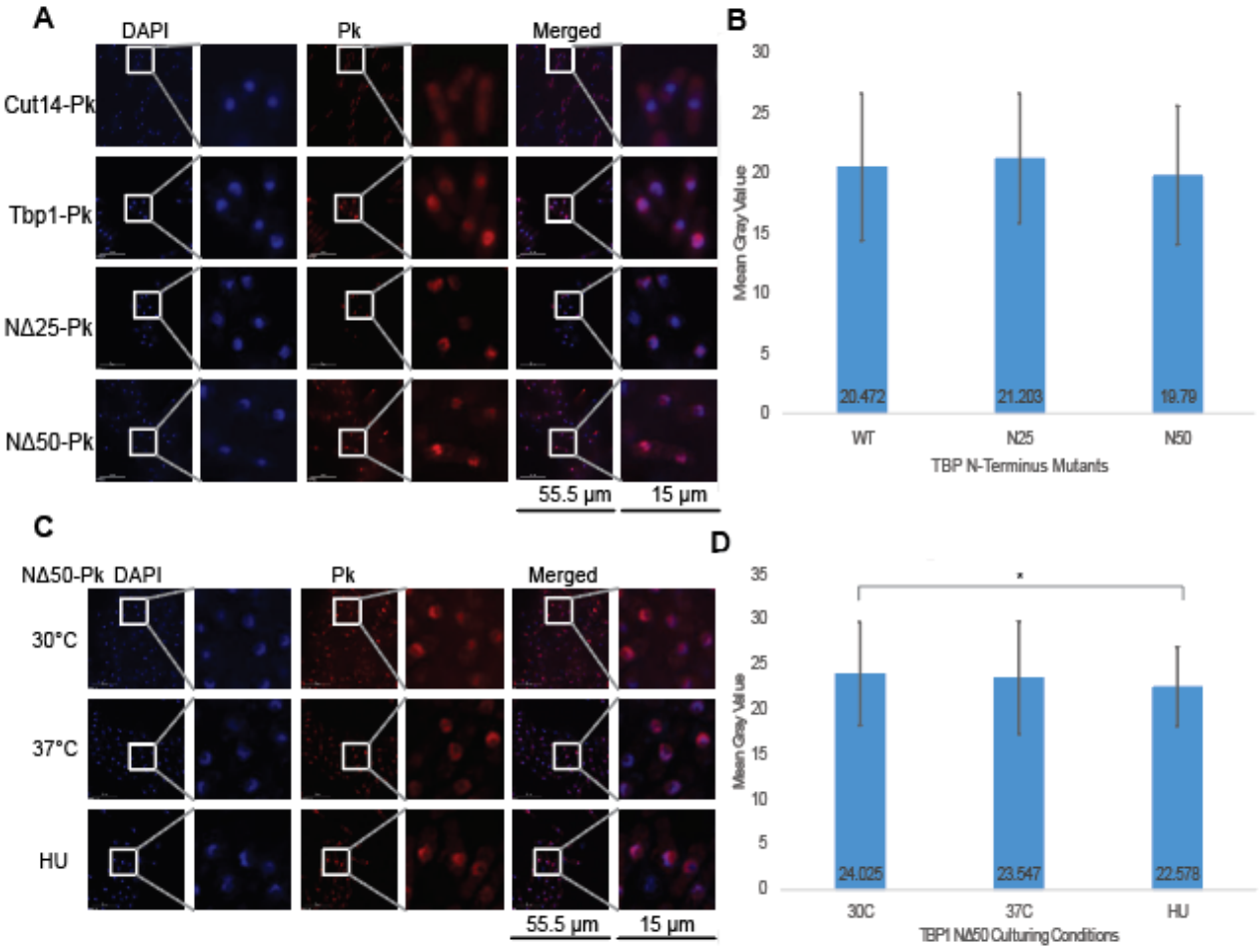
A
DAPI
Pk
Merged
Cut14-Pk
Tbp1-Pk
NΔ25-Pk
NΔ50-Pk
55.5 µm
15 µm
B
Mean Gray Value
30
25
20
15
10
5
0
20.472
21.203
19.79
WT
N25
N50
TBP N-Terminus Mutants
C
NΔ50-Pk DAPI
Pk
Merged
30°C
37°C
HU
55.5 µm
15 µm
D
Mean Gray Value
35
30
25
20
15
10
5
0
*
24.025
23.547
22.578
30C
37C
HU
TBP1 NΔ50 Culturing Conditions
E
DAPI
TAT-1
Cnd2
Merged
WT
WT
NΔ50
NΔ50
55.5 µm
15 µm

Figure 7. Localization of TBP and TBP-NΔ proteins. Representative IF images show the TBP WT and NΔ proteins tagged with Pk (red) and DAPI signals (blue). (A) TBP-WT-Pk cells displayed a bright Pk signal concentrated in nuclei, similar to the TBP-NΔ-Pk strains. (B) Mean gray value indicative of signal intensity of the TBP-WT and NΔ strains. Data is presented as mean +/- standard deviation (error bar). No significant differences in nuclear intensity were found between the TBP-WT and NΔ cells. (C) TBP-NΔ50-Pk cells were visualized under several culturing conditions: 30°C (control), 37°C, and 5% hydroxyurea (HU). (D) Mean gray value (intensity) of TBP-NΔ50-Pk cells cultured in 30°C, 37°C, and 5% HU. Data is presented as mean +/- standard deviation (error bar). TBP-NΔ50-Pk cells cultured in 5% HU displayed a significantly lower mean gray value compared to the 30°C control condition (p=0.013)*. (E) Representative IF images show DAPI staining (blue) and localization of Cnd2 condensin (green) and TAT-1 tubulin (red) in the TBP-WT-Pk and NΔ50-Pk strains. Strong nuclear Cnd2 signals and spindles reflect mitotic cells.

	# of cells with strong Cnd2 signals	# of cells with TAT-1 signals	# of cells with TAT-1 nuclear signals	# of cells with TAT-1 line signals
WT	8	8 (100%)	4 (50%)	4 (50%)
NΔ50	9	9 (100%)	5 (55.6%)	4 (44.4%)

Table 1. Quantification of signals present in IF images during mitosis. Both the TBP-WT and NΔ50 strains displayed similar signal localizations.

Varying concentrations of HD affect the localization of TBP-WT and NΔ50 proteins

Given the potential influence of 1,6-hexanediol (HD) on the cellular environment and DNA regulation (Jones & Forsburg, 2023), I hypothesized that HD exposure might affect the behavior of the TBP-WT and NΔ proteins. Particularly, the N-terminus likely plays a crucial role in mediating protein-protein interactions and could thereby affect the phase separation propensity of TBP complexes. To examine the potential effects, TBP-WT-Pk and NΔ50-Pk strains were cultured in different HD concentrations ranging from 0 to 9% and visualized through IF microscopy (Fig. 8). Under 5% HD, which included 1.25% HD, and 2.5% HD, there were no significant visual differences between the TBP-WT-Pk and NΔ50-Pk strains. Additionally, concentrations of HD under 5% did not significantly affect TBP localization, thus both TBP-WT-Pk and NΔ50-Pk both resembled their counterparts without HD. Specifically, nearly all cells displayed bright nuclear Pk signals (Fig. 8A). Quantitative analysis revealed a notable influence

of HD on both TBP-WT-Pk and NΔ50-Pk cells, as evidenced by a decreasing percentage of cells displaying bright nuclear signals with increasing HD concentration (Table 2). Notably, at HD concentrations ranging from 6% to 9%, both the TBP-WT-Pk and NΔ50-Pk strains exhibited sensitivity to HD. Nonetheless, even at these higher HD concentrations, some cells retained bright nuclear TBP signals (Fig. 8B). Quantification corroborated these observations, demonstrating a decrease in the percentage of cells with nuclear signals and a concurrent increase in the proportion of cells lacking Pk signals as HD concentration increased from 6% to 9% (Table 2). Interestingly, TBP-WT-Pk cells exhibited heightened sensitivity to HD compared to TBP-NΔ50-Pk cells. Moreover, at an HD concentration of 7%, the most substantial difference in the percentage of cells displaying bright nuclear signals was observed. Consequently, further analysis of TBP-WT-Pk and NΔ50-Pk cells was conducted at the HD concentration of 7%.

Further examination of the TBP-WT-Pk and NΔ50-Pk strains cultured in 7% HD confirmed distinct sensitivity patterns between the two strains. In both strains, three distinct Pk signaling patterns were observed: bright nuclear signal, dispersed pattern, and low to no signal (Fig. 8C). In TBP-WT-Pk cells, exposure to 7% HD resulted in a pronounced decrease in the percentage of cells exhibiting bright nuclear signals compared to untreated TBP-WT cells. Visually, a significant proportion of TBP-WT-Pk cells displayed diminished Pk signals or were devoid of nuclear staining altogether, indicating a heightened sensitivity to HD-induced stress. Conversely, TBP-NΔ50-Pk cells exhibited a comparatively milder response to 7% HD exposure. While some reduction in the percentage of cells with bright nuclear signals was observed, a substantial fraction of TBP-NΔ50-Pk cells still retained detectable Pk signals within the nucleus, albeit at lower intensity levels compared to untreated conditions (Fig. 8C). Quantitative analysis corroborated these qualitative observations, revealing a more pronounced decreased in the

percentage of TBP-WT-Pk cells with bright nuclear signals compared to TBP-NΔ50-Pk cells under 7% HD treatment (Fig. 8D). Similarly, there was also an increase in the percentage of TBP-WT-Pk cells exhibiting low Pk signals compared to TBP-NΔ50-Pk cells under 7% HD treatment (Fig. 8D). Statistical differences were found between the TBP-WT-Pk and NΔ50-Pk strains in the cell populations showing low TBP signals ($p=0.006$)** or nuclear signals ($p=0.006$)**. These findings underscored the distinct sensitivity of TBP-WT-Pk and NΔ50-Pk cells to HD-induced stress, with TBP-WT-Pk cells displaying heightened susceptibility to HD-mediated perturbations in nuclear Pk localization compared to TBP-NΔ50-Pk cells.

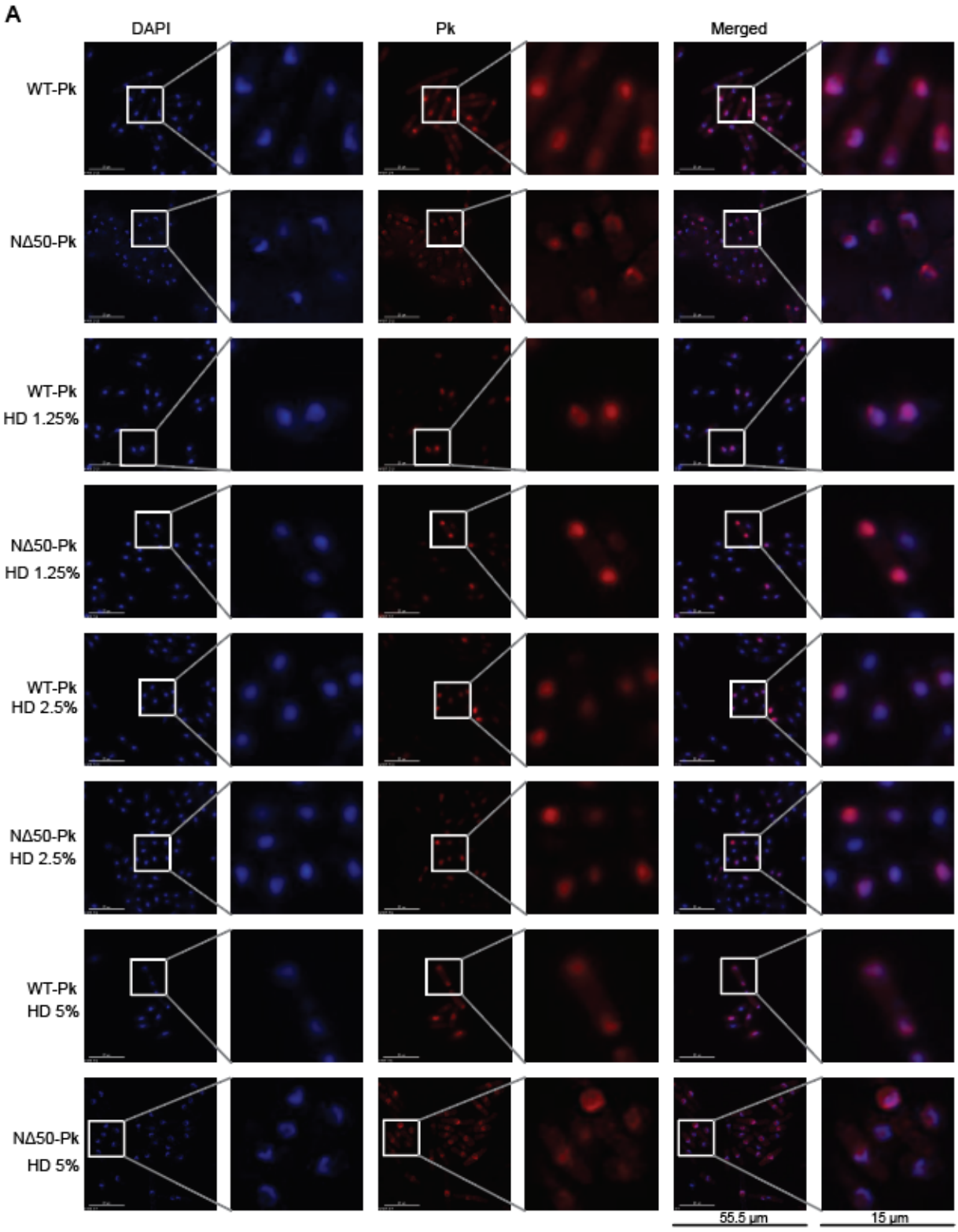
A
DAPI
Pk
Merged
WT-Pk
NΔ50-Pk
WT-Pk
HD 1.25%
NΔ50-Pk
HD 1.25%
WT-Pk
HD 2.5%
NΔ50-Pk
HD 2.5%
WT-Pk
HD 5%
NΔ50-Pk
HD 5%
55.5 µm
15 µm

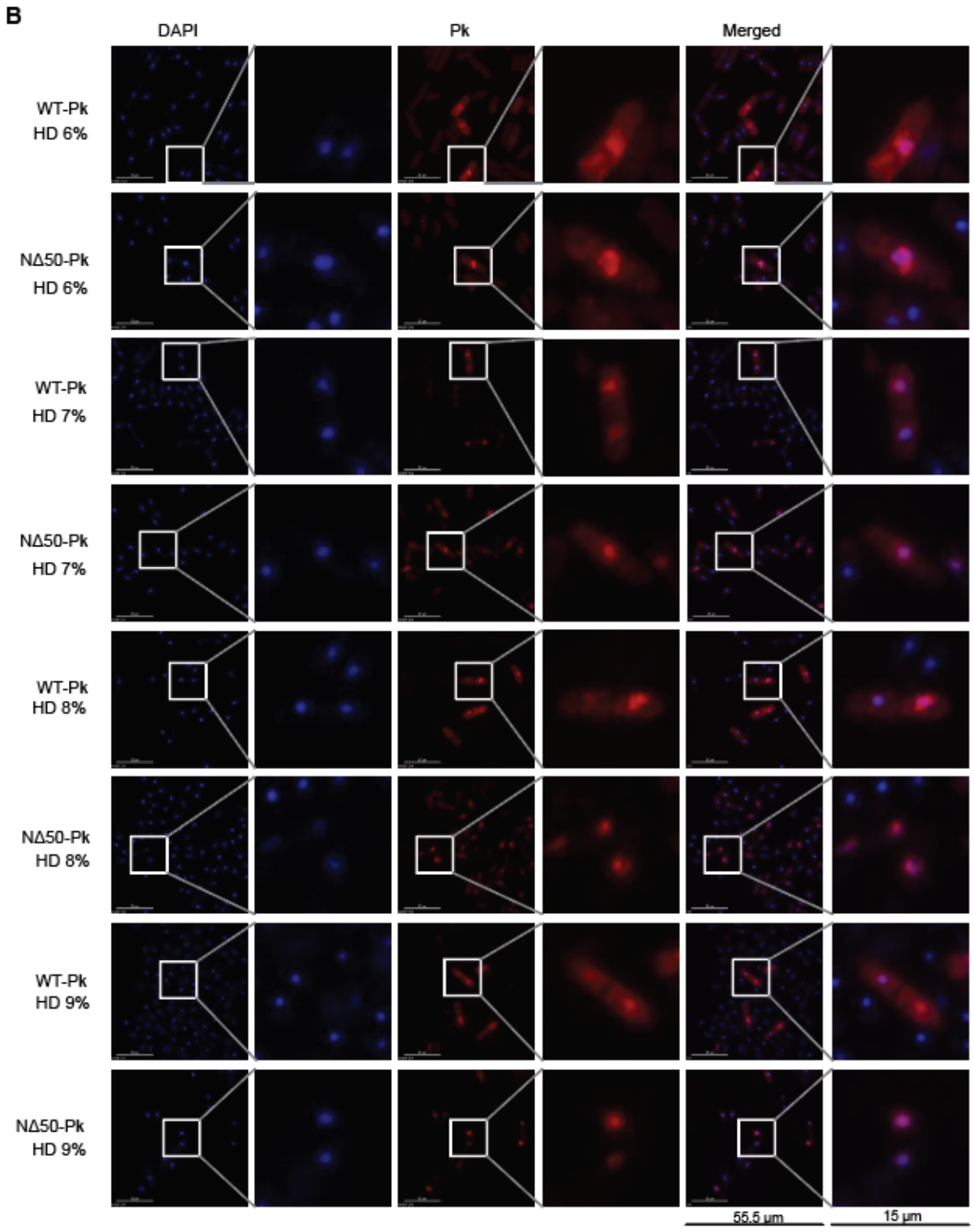
B
DAPI
Pk
Merged
WT-Pk
HD 6%
NΔ50-Pk
HD 6%
WT-Pk
HD 7%
NΔ50-Pk
HD 7%
WT-Pk
HD 8%
NΔ50-Pk
HD 8%
WT-Pk
HD 9%
NΔ50-Pk
HD 9%
55.5 μm
15 μm

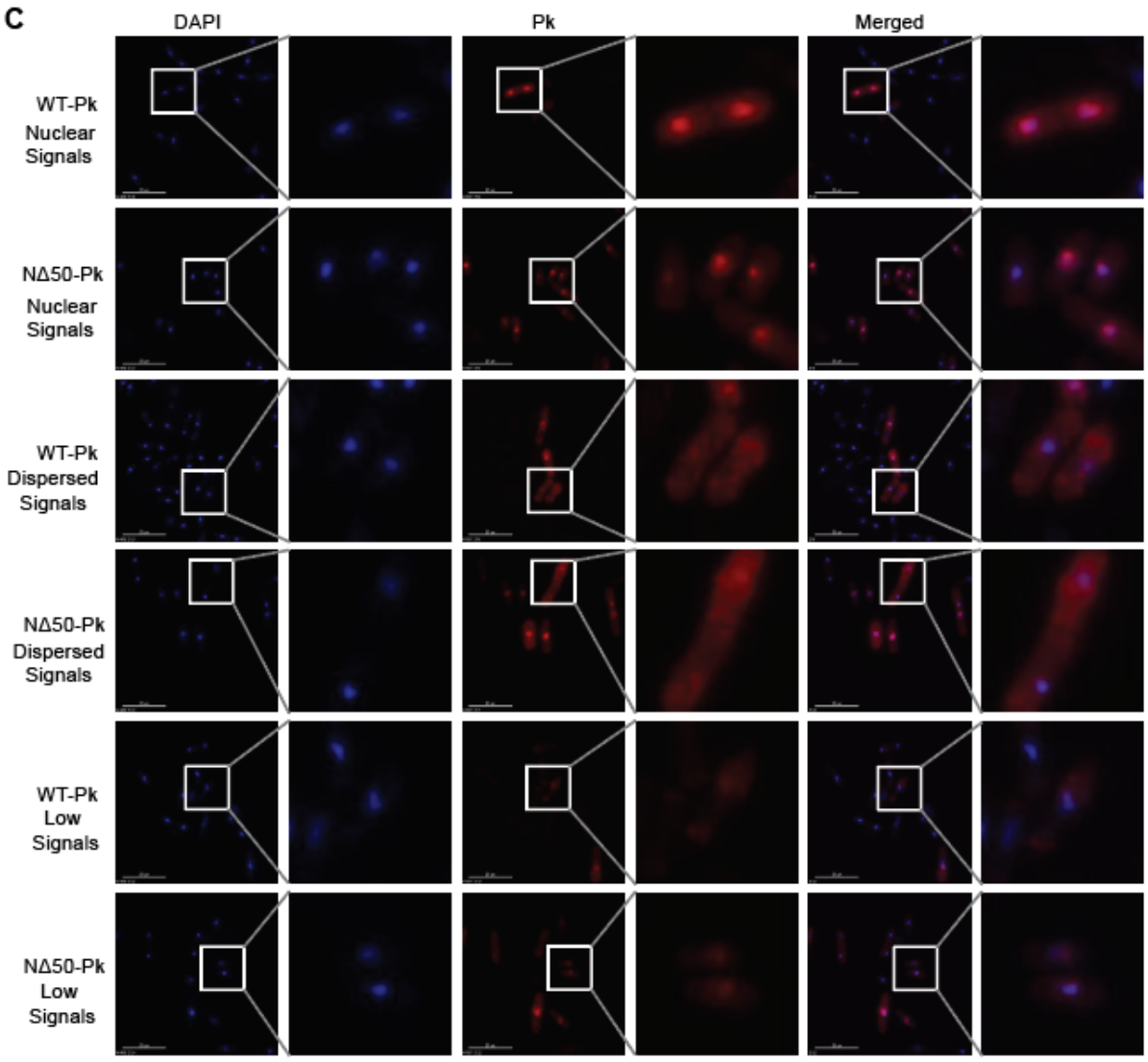
C
DAPI
Pk
Merged
WT-Pk Nuclear Signals
NΔ50-Pk Nuclear Signals
WT-Pk Dispersed Signals
NΔ50-Pk Dispersed Signals
WT-Pk Low Signals
NΔ50-Pk Low Signals

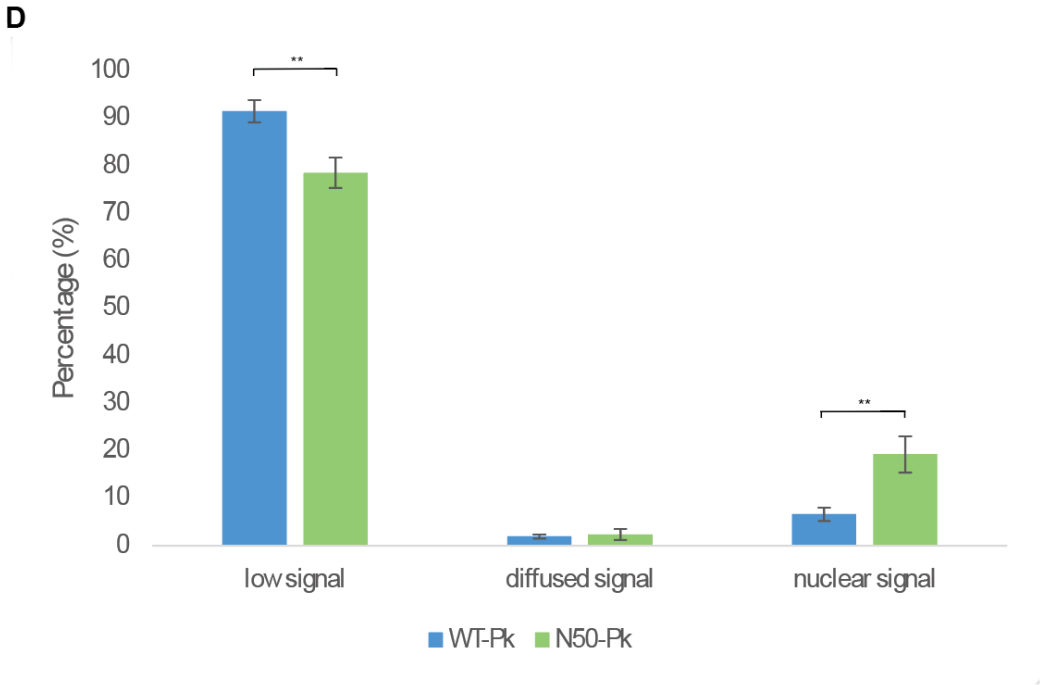

Figure 8. Immunofluorescence (IF) images showed distinct sensitivity patterns between TBP-WT-Pk and NΔ50-Pk cells. (A) Representative IF images depicting Pk signaling (red) in TBP-WT-Pk and NΔ50-Pk cells under varying hydroxyurea (HD) concentrations: 0%, 1.25%, 2.5%, and 5%. (B) IF images showing Pk signals in TBP-WT-Pk and NΔ50-Pk cells exposed to higher HD concentrations: 6%, 7%, 8%, and 9%. (C) IF images show three distinct Pk signal patterns observed in cells treated with 7% HD: cells with bright nuclear signals, cells with dispersed Pk signals, and cells with low Pk signals. (D) Quantification of IF images at 7% HD. Cells were categorized into three Pk signal groups: low signal, diffused signal, and nuclear signal. Data presented as mean +/- standard deviation (error bar). Statistical differences were found between the TBP-WT-Pk and NΔ50-Pk strains in the cell populations showing low TBP signals (p=0.006)** or nuclear signals (p=0.006)**.

	LOW SIGNAL	DIFFUSED SIGNAL	NUCLEAR SIGNAL	TOTAL (#)
WT-PK	25 (8.8%)	312 (11.0%)	228 (80.3%)	284
NΔ50-PK	27 (9.0%)	29 (9.6%)	245 (81.4%)	301
WT-PK HD 1.25%	23 (14%)	16 (9.8%)	125 (76.2%)	164
NΔ50-PK HD 1.25%	16 (10.5%)	18 (11.8%)	119 (77.8%)	153
WT-PK HD 2.5%	26 (13.9%)	23 (12.3%)	138 (73.8%)	187
NΔ50-PK HD 2.5%	20 (14.8%)	15 (11.1%)	100 (74.1%)	135
WT-PK HD 5%	36 (24.2%)	21 (14.0%)	92 (61.7%)	149
NΔ50-PK HD 5%	42 (25.9%)	17 (10.5%)	103 (63.6%)	162
WT-PK HD 6%	216 (91.9%)	16 (6.8%)	3 (1.3%)	235
NΔ50-PK HD 6%	110 (88.7%)	7 (5.6%)	7 (5.6%)	124
WT-PK HD 7%	157 (93.5%)	3 (1.8%)	8 (4.8%)	168
NΔ50-PK HD 7%	106 (82.8%)	4 (3.9%)	18 (14.1%)	128
WT-PK HD 8%	136 (92.5%)	3 (2.0%)	8 (5.4%)	147
NΔ50-PK HD 8%	100 (84.7%)	14 (11.9%)	4 (3.4%)	118
WT-PK HD 9%	107 (94.7%)	3 (2.7%)	3 (2.7%)	113
NΔ50-PK HD 9%	85 (82.5%)	3 (2.9%)	8 (4.8%)	168

Table 2. Quantification of Pk signals in the TBP-WT-Pk and NΔ50-Pk strains under various HD concentrations. TBP-WT-Pk and NΔ50-Pk cells both exhibited cells with the three distinct Pk signal patterns: low signal, diffused signal, and nuclear signal. Notably, at 7% HD (highlighted in yellow), the most substantial difference in the percentage of cells displaying nuclear signals was observed.

Next-generation sequencing (NGS) technology revealed alterations in TBP-NΔ gene expression, binding, and gene domains

Our initial hypothesis was that the TBP-NΔ strains might display lower gene expression levels due to the observed decrease in growth rates. To test this hypothesis, RNA-seq data was

analyzed to assess how gene expression was affected across the chromosome in these mutants. Analysis of the RNA-seq data unveiled distinct patterns of gene expression alterations between the TBP WT and NΔ strains (Fig. 9A). In this experiment, both input and nascent (biotin) RNA was analyzed, with input RNA being the total pool of cellular RNA and nascent RNA being RNA that were newly transcribed (Wissink et al., 2019). Specifically, genes were generally downregulated in TBP-NΔ50 cells compared to TBP-WT cells in both input and biotin samples, suggesting a global reduction in transcriptional level in these mutants. Conversely, TBP-NΔ25 cells exhibited gene expression profiles that were largely similar to TBP-WT cells, albeit with slight downregulation in some genes. Interestingly, despite the prevailing trend of gene downregulation in TBP-NΔ50 cells, a subset of genes showed significant upregulation compared to TBP-WT cells (Fig. 9B and Table 3). This unexpected observation highlights the complexity of the regulatory mechanisms governing gene expression in the TBP-NΔ mutants and underscores the need for further investigation into the underlying molecular pathways driving these differential expression patterns.

Analysis of chromatin immunoprecipitation followed by high-throughput sequencing (ChIP-seq) data was conducted to investigate the binding activity of the TBP WT and NΔ proteins across the genome. The data revealed that, for the most part, TBP binding was retained in the TBP-NΔ strain, indicating that the TBP-NΔ mutations do not abolish TBP binding to chromatin (Fig. 9C). However, notable differences in binding activity were observed between the TBP-WT and NΔ proteins, particularly in the case of the TBP-NΔ50 protein. While binding activity remained largely consistent between the TBP-WT and NΔ25 proteins, a subset of genes exhibited significantly increased binding of the TBP–NΔ50 proteins compared to the TBP-WT protein (Fig. 9D and Table 4). The identification of genes with increased binding of the TBP-

NΔ50 protein provides valuable insights into the potential regulatory roles of the N-terminal domain in modulating TBP binding dynamics and gene expression.

A comparative analysis of RNA-seq and ChIP-seq data revealed intriguing associations between gene expression levels and TBP binding activity across the genome. Notably, there were several genes in the TBP-NΔ50 strain that exhibited concurrent upregulation in RNA-seq data and increased TBP binding activity in ChIP-seq data. Two such notable genes include hsp9 and hsp16, which displayed elevated expression levels in RNA-seq data and concomitant enhancement in TBP binding activity in ChIP-seq data (Fig. 9B and 9D). An additional gene that also displayed this trend includes gpd3, known for its role in the glycolytic pathway during oxidative stress response (Papadakis & Workman, 2014). The upregulation of the heat shock protein genes, hsp9 and hsp16, are known for their roles in cellular stress response mechanisms, suggesting a potential regulatory role in TBP binding in modulating their expression levels (Cabrera et al., 2020). The convergence of findings from RNA-seq and ChIP-seq data highlights the interplay between transcriptional regulation and TBP binding dynamics, underscoring the importance of TBP in orchestrating gene expression programs involved in stress response pathways.

In addition to RNA-seq and ChIP-seq data, I integrated Hi-C data to explore the spatial organization of chromatin and its relationship with gene expression and TBP binding activity. Specifically, I examined Hi-C heatmaps focusing on genomic regions corresponding to genes that exhibited upregulation in RNA-seq data and concurrent increases in TBP binding in ChIP-seq data. Interestingly, the analysis revealed no significant visual disruptions in the formation of gene domains at the region of hsp9, suggesting that the observed changes in gene expression and TBP binding activity were not accompanied by pronounced alterations in chromatin structure at

these loci (Fig. 10A). However, local Hi-C heatmaps at the region of hsp16 showed decreased interaction within the chromosome, suggesting a disruption in the formation of gene domains (Fig. 10B).

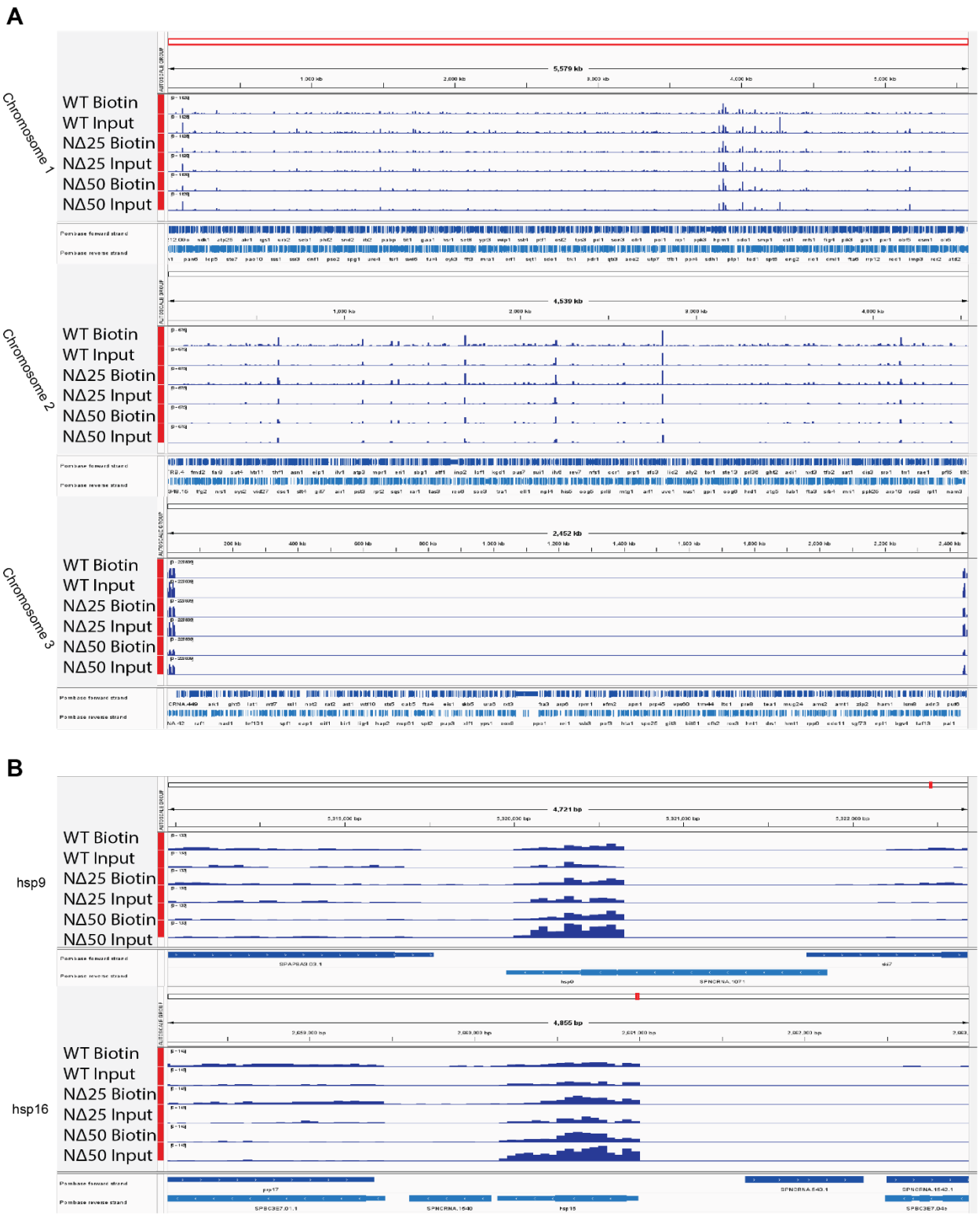
A
Chromosome 1
WT Biotin
WT Input
NΔ25 Biotin
NΔ25 Input
NΔ50 Biotin
NΔ50 Input
Chromosome 2
WT Biotin
WT Input
NΔ25 Biotin
NΔ25 Input
NΔ50 Biotin
NΔ50 Input
Chromosome 3
WT Biotin
WT Input
NΔ25 Biotin
NΔ25 Input
NΔ50 Biotin
NΔ50 Input
B
hsp9
WT Biotin
WT Input
NΔ25 Biotin
NΔ25 Input
NΔ50 Biotin
NΔ50 Input
hsp16
WT Biotin
WT Input
NΔ25 Biotin
NΔ25 Input
NΔ50 Biotin
NΔ50 Input

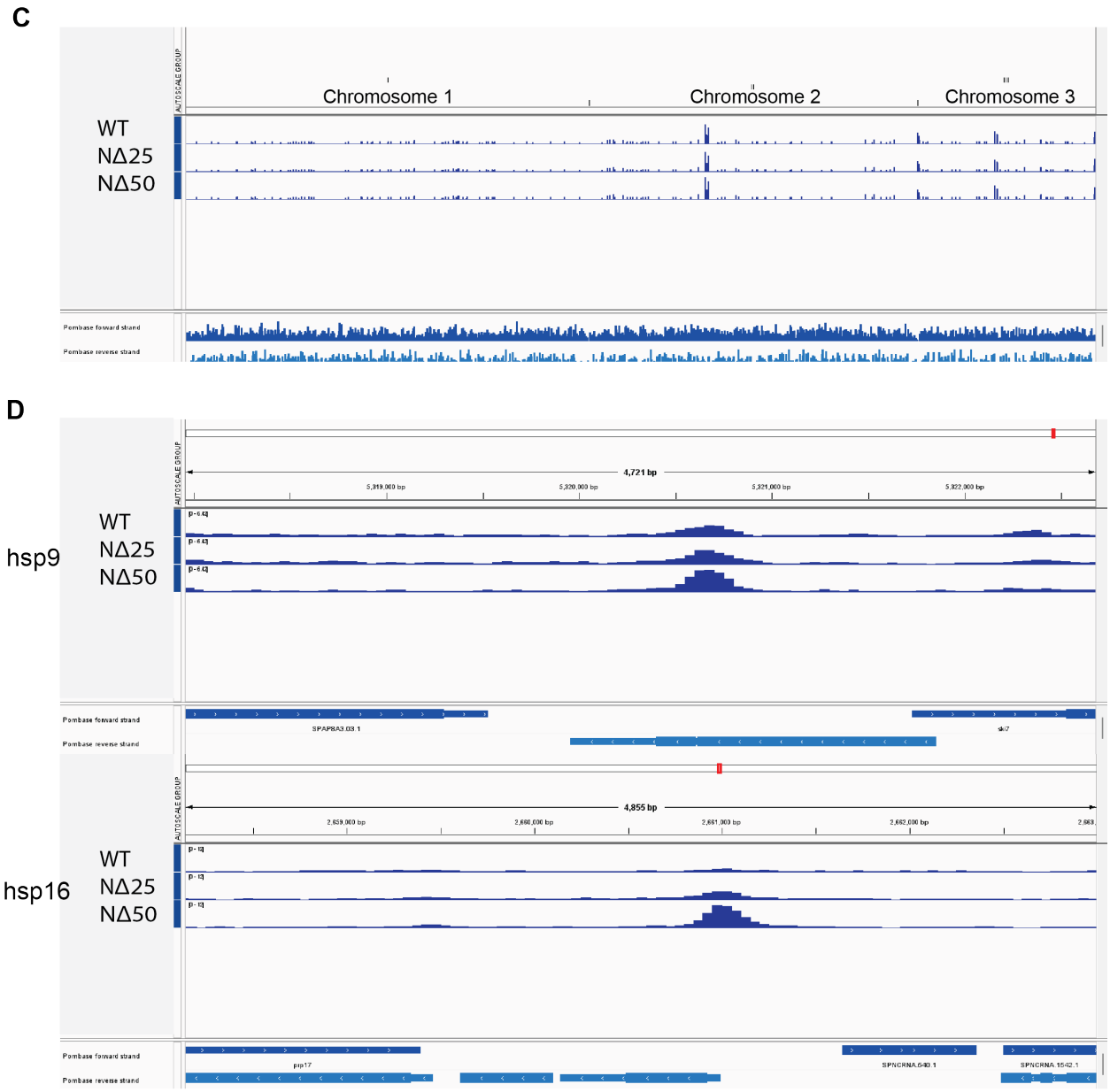

Figure 9. Integrated analysis of RNA-seq and ChIP-seq data reveals dynamic regulatory relationships governing gene expression and TBP binding in WT and TBP-NΔ mutant strains. Both input and nascent (biotin) RNA-seq is shown for all samples. (A) RNA-seq data depicting genome-wide gene expression profiles in the TBP-WT, NΔ25, and NΔ50 strains, with a substantial portion of genes in TBP-NΔ50 cells showing downregulation compared to WT cells. (B) RNA-seq data depicting hsp9 and hsp16, highlighting their upregulation in TBP-NΔ50 mutant. (C) ChIP-seq data mapping TBP binding across the genome for TBP-WT, NΔ25, and NΔ50 strains, showing that most binding is retained in the TBP-NΔ mutants compared to WT. (D) ChIP-seq data depicting hsp9 and hsp16 revealed increased TBP binding, particularly in the TBP-NΔ50 strain.

Chromosome (number of genes)	List of genes upregulated in TBPNΔ50 cells predicted from RNA-seq data
Chromosome 1 (16)	Rgs1
	Prz1
	SPAC343.20
	SPAC4G9.22.1
	SPAC22H10.13.1
	SPAC23H3.15C.1
	SPAC4A8.04.1
	SPAPB24D3.07c.1
	Bgl2
	SPAC29E6.08.1
	Mei2
	Omt3
	SPAC637.03.1
	Hsp9
	SPAC869.05c
	Yhb1
Chromosome 2 (14)	SPBPB21E7.04c.1
	SPBPB21E7.08.1.
	SPBC660.05
	SPBC660.06
	Adh8
	SPNCRNA.103.1
	Gpd3
	SPNCRNA.322.1
	SPBC1E8.05
	SPBC29A10.08.1
	Hsp16
	SPBC19C7.04c.1
	SPBC1105.05.1
	SPBC32C12.02.1
Chromosome 3 (1)	Ctt1

Table 3. Summary of genes that are upregulated in TBPNΔ50 mutants compared to WT cells based on RNA-seq data. Highlighted genes indicate those that exhibit concurrent upregulation in RNA-seq and increased TBP binding in ChIP-seq data. This table provides insights into potential candidate genes regulated by TBP and affected by TBPNΔ mutations.

Chromosome (number of genes)	List of genes with increased TBP binding in TBPNΔ50 cells predicted from ChIP-seq data
Chromosome 1 (23)	SPRPTA.6 SPRPTA.8 Mfs2 Asl1 SPAC24B11.06c.1 SPNCRNA.625.1 SPAC821.10c.1 Met9 Cdc48 SPNCRNA.811.1 SPAC22H10.13.1 Rif1 SPAC513.07 SPNCRNA.863 SPAPB24D3.07c.1 SPAC1786.02.1 Mg10 SPAC15A10.02.1 SPAC1071.10c.1 SPAC29E6.08.1 Met14 Hsp9 Ftm4
Chromosome 2 (26)	SPBPB8B6.05c SPBC354.06.1 Gpd3 SPNCRNA.1379.1 SPBC119.08.1 Ubi4 SPNCRNA.1409 But2 SPBC3H7.02.1 SPNCRNA.1487.1 SPBC36B7.08c.1 SPBC29A10.08.1 Hsp16 SPNCRNA.419.1 Lys4 SPBC1105.05.1 Hsp104 Pop7 SPBC19F5.04.1 Snu32 Arg4 SPNCRNA.1672.1 Pan5 SPRPTB.13 Mmf1 SPBPB7E8.01
Chromosome 3 (12)	CU329672_gene_group_5542…13722 SPNCRNA.1096.1 SPCC330.03c.1 Srp68 Rpl35a

	Sti1
	SPCC23B6.01c.1
	SPNCRNA.1187.1
	Wss2
	SPCC1739.10.1
	SPCC1739.13.1
	SPCC1620.11.1

Table 4. Summary of genes that have increased TBP binding in the TBP-NΔ50 mutant compared to WT cells based on ChIP-seq data. Highlighted genes indicate those that exhibit concurrent upregulation in RNA-seq and increased TBP binding in ChIP-seq data. This table provides insights into potential candidate genes of TBP whose binding is notably enhanced in the presence of the TBPNΔ mutation, shedding light on the regulatory roles of TBP and the impact of the TBPNΔ alterations on chromatin binding dynamics.

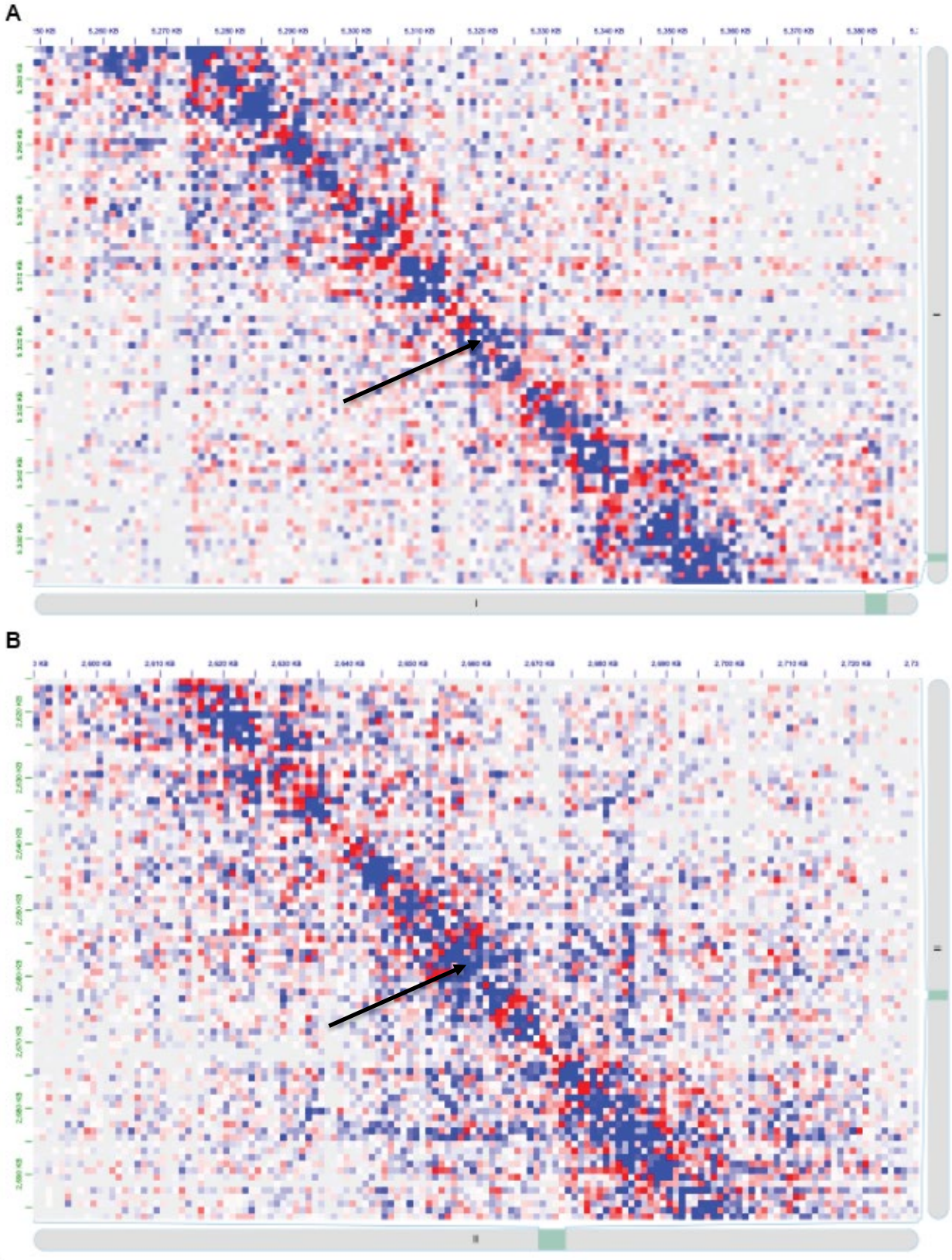
A
B

Figure 10. Local Hi-C maps showed some alterations in the formation of gene domains. Red indicates increased chromatin interaction frequencies, while blue indicates decreased chromatin interaction frequencies. (A) Local Hi-C map focusing on the hsp9 gene in chromosome 1. (B) Local Hi-C map focusing on the hsp16 gene in chromosome 2.

Discussion

The comprehensive investigation into the role of the TBP N-terminal region in gene domain formation, stress responses, and cellular physiology in fission yeast presents a multifaceted understanding of transcriptional regulation and genome organization. The experimental approach, encompassing genetic manipulations, phenotypic assays, microscopy, and high-throughput sequencing analyses, offers a holistic view of the molecular mechanisms underlying TBP-mediated cellular processes. The results provide valuable insights into the functional significance of the N-terminal domain of TBP, shedding light on its role in shaping transcriptional landscapes, modulating nuclear morphology, and orchestrating stress responses.

The observed alterations in growth rates and sensitivity profiles of TBP-NΔ mutants underscore the critical role of the N-terminal region in cellular fitness and stress adaptation. The significant increase in doubling time exhibited by TBP-NΔ50 mutants, particularly under heat stress and exposure to hydroxyurea, highlights the importance of this domain in mediating stress responses. Interestingly, the rescue of growth phenotypes by the incorporation of Pk epitope tags, especially at the N-terminal end, suggests potential regulatory roles of these tags in mitigating the deleterious effects of TBP-N-terminal deletions. This finding raises intriguing questions regarding the mechanisms underlying the rescue effects of Pk tags and warrants further investigation into the functional implications of tag position on protein behavior and cellular physiology.

Microscopic analysis of nuclear morphology reveals distinct alterations in nuclear shape and size in TBP-NΔ mutants, particularly in TBP-NΔ50 strains. The observed crescent-shaped nuclei hint at potential disruptions in nuclear processes, such as transcription and DNA replication, underpinning the observed growth defects. However, the rescue of nuclear

morphology in TBP-NΔ50-Pk strains suggests modulatory effects of Pk tags on nuclear organization, emphasizing the importance of considering tag position in future studies. Furthermore, immunofluorescent microscopy provides valuable insights into TBP localization dynamics under different culturing conditions, with subtle changes observed in TBP distribution under stress conditions, particularly in the presence of HD. In particular, comparison under 7% HD exposure showed TBP-WT-Pk cells as more sensitive to HD-induced stress with a pronounced decreased in cells displaying bright nuclear signals compared to TBP-NΔ50-Pk cells, suggesting a phase separation mechanism in nuclear TBP localization. These findings underscore the dynamic nature of TBP localization and hint at potential regulatory roles of the N-terminal domain in modulating TBP localization dynamics during stress responses.

Moreover, examination of TBP-NΔ mutants during mitosis reveals conserved tubulin localization patterns between WT and mutant strains, suggesting that N-terminal deletions do not disrupt mitotic spindle formation or chromosome condensation. These findings highlight the robustness of TBP-mediated mitotic processes and underscore its importance in coordinating chromosome dynamics during cell division. Integration of next-generation sequencing technologies provides deeper insights into the molecular mechanisms underlying the observed phenotypic changes in TBP-NΔ mutants. RNA-seq analysis unveils distinct alterations in gene expression profiles, with TBP-NΔ50 mutants exhibiting global downregulation of transcriptional activity compared to WT. Concurrent ChIP-seq analysis reveals differential binding activity of TBP-NΔ mutants across the genome, particularly in TBP-NΔ50 strains, suggesting complex regulatory interactions between the N-terminal domain and chromatin.

Of particular interest are the findings regarding the upregulation of heat shock protein genes, such as hsp9 and hsp16, in TBP-NΔ mutants. The concurrent increase in expression levels

of these genes, known for their roles in cellular stress response mechanisms, hints at potential regulatory roles of TBP binding in modulating their expression levels. The convergence of findings from RNA-seq and ChIP-seq data underscores the interplay between transcriptional regulation and TBP binding dynamics, highlighting the importance of TBP in orchestrating gene expression programs involved in stress response pathways. This observation raises intriguing possibilities regarding the molecular mechanisms underlying heat stress responses and warrants further investigation into the functional significance of TBP-mediated regulation of heat shock protein genes. Additionally, the local Hi-C maps revealed possible disruptions in the chromatin structure around the hsp16 gene, likely interfering with proper gene domain formation and regulation. This disruption may result in misexpression of hsp16, impairing the heat shock response and leading to lower viability in temperature-sensitive growth assays. However, Hi-C maps at much higher resolution are necessary to better define the alternations in gene domains at these gene loci. These findings suggest that chromatin structure architecture, specifically gene domains, plays a critical role in gene regulation and stress response, explaining the phenotypic sensitivity to elevated temperatures.

Overall, the comprehensive study provides a nuanced understanding of the role of the TBP N-terminal domain in transcriptional regulation, genome organization, and stress responses in fission yeast. The findings underscore the functional significance of this domain in shaping cellular physiology and highlight the complex regulatory networks governing TBP-mediated cellular processes. Further investigations into the molecular mechanisms underlying TBP-NΔ mutant phenotypes hold promise for uncovering novel insights into transcriptional regulation and stress adaptation mechanisms in eukaryotic cells.

Bibliography

Alao, J. P., Weber, A. M., Shabro, A., & Sunnerhagen, P. (2015). Suppression of sensitivity to drugs and antibiotics by high external cation concentrations in fission yeast. PLOS ONE, 10(3). https://doi.org/10.1371/journal.pone.0119297

Anandapadamanaban, M., Andresen, C., Helander, S., Ohyama, Y., Siponen, M. I., Lundström, P., Kokubo, T., Ikura, M., Moche, M., & Sunnerhagen, M. (2013). High-resolution structure of TBP with taf1 reveals anchoring patterns in transcriptional regulation. Nature Structural & Molecular Biology, 20(8), 1008–1014. https://doi.org/10.1038/nsmb.2611

Boija, A., Klein, I. A., Sabari, B. R., Dall'Agnese, A., Coffey, E. L., Zamudio, A. V., Li, C. H., Shrinivas, K., Manteiga, J. C., Hannett, N. M., Abraham, B. J., Afeyan, L. K., Guo, Y. E., Rimel, J. K., Fant, C. B., Schuijers, J., Lee, T. I., Taatjes, D. J., & Young, R. A. (2018). Transcription factors activate genes through the phase-separation capacity of their activation domains. Cell, 175(7). https://doi.org/10.1016/j.cell.2018.10.042

Cabrera, M., Boronat, S., Marte, L., Vega, M., Pérez, P., Ayté, J., & Hidalgo, E. (2020). Chaperone-facilitated aggregation of thermo-sensitive proteins shields them from degradation during heat stress. Cell Reports, 30(7). https://doi.org/10.1016/j.celrep.2020.01.077

Carter, R., & Drouin, G. (2009). Structural differentiation of the three eukaryotic RNA polymerases. Genomics, 94(6), 388–396. https://doi.org/10.1016/j.ygeno.2009.08.011

Chatterjee, S., & Struhl, K. (1995). Connecting a promoter-bound protein to TBP bypasses the need for a transcriptional activation domain. Nature, 374(6525), 820–822. https://doi.org/10.1038/374820a0

Cobb, M. (2017). 60 years ago, Francis Crick changed the logic of Biology. PLOS Biology, 15(9). https://doi.org/10.1371/journal.pbio.2003243

Collura, A., Blaisonneau, J., Baldacci, G., & Francesconi, S. (2005). The fission yeast crb2/chk1 pathway coordinates the DNA damage and spindle checkpoint in response to replication stress induced by topoisomerase I inhibitor. Molecular and Cellular Biology, 25(17), 7889–7899. https://doi.org/10.1128/mcb.25.17.7889-7899.2005

Davidson, I. (2003). The genetics of TBP and TBP-related factors. Trends in Biochemical Sciences, 28(7), 391–398. https://doi.org/10.1016/s0968-0004(03)00117-8

Hayles, J., & Nurse, P. (2017). Introduction to fission yeast as a model system. Cold Spring Harbor Protocols, 2018(5). https://doi.org/10.1101/pdb.top079749

Hernandez, N. (1993). TBP, a universal eukaryotic transcription factor? Genes & Development, 7(7b), 1291–1308. https://doi.org/10.1101/gad.7.7b.1291

Hobbs, N. K., Bondareva, A. A., Barnett, S., Capecchi, M. R., & Schmidt, E. E. (2002). Removing the vertebrate-specific TBP N terminus disrupts placental B2M-dependent interactions with the maternal immune system. Cell, 110(1), 43–54. https://doi.org/10.1016/s0092-8674(02)00806-1

Hsieh, T.-H. S., Fudenberg, G., Goloborodko, A., & Rando, O. J. (2016). Micro-C XL: Assaying Chromosome Conformation at Length Scales from the Nucleosome to the Entire Genome. https://doi.org/10.1101/071357

Iwasaki, O., Tanizawa, H., Kim, K.-D., Yokoyama, Y., Corcoran, C. J., Tanaka, A., Skordalakes, E., Showe, L. C., & Noma, K. (2015). Interaction between TBP and condensin drives the organization and faithful segregation of mitotic chromosomes. Molecular Cell, 59(5), 755–767. https://doi.org/10.1016/j.molcel.2015.07.007

Jerkovic´, I., & Cavalli, G. (2021). Understanding 3D genome organization by multidisciplinary methods. Nature Reviews Molecular Cell Biology, 22(8), 511–528. https://doi.org/10.1038/s41580-021-00362-w

Jones, C. E., & Forsburg, S. L. (2023). Impact of 1,6-hexanediol on schizosaccharomyces pombe genome stability. G3: Genes, Genomes, Genetics, 13(8). https://doi.org/10.1093/g3journal/jkad123

Kim, Y., Geiger, J. H., Hahn, S., & Sigler, P. B. (1995). Crystal Structure of a Yeast TBP/TATA-Box Complex. https://doi.org/10.2210/pdb1ytb/pdb

Kuddus, R., & Schmidt, M. C. (1993). Effect of the non-conserved N-terminus on the DNA binding activity of the yeast tata binding protein. Nucleic Acids Research, 21(12), 2962–2962. https://doi.org/10.1093/nar/21.12.2962-a

Lee, T. I., & Young, R. A. (1998). Regulation of gene expression by TBP-associated proteins. Genes & Development, 12(10), 1398–1408. https://doi.org/10.1101/gad.12.10.1398

Lescure, A., Lutz, Y., Eberhard, D., Jacq, X., Krol, A., Grummt, I., Davidson, I., Chambon, P., & Tora, L. (1994). The N-terminal domain of the human TATA-binding protein plays a role in transcription from TATA-containing RNA polymerase II and III promoters. The EMBO Journal, 13(5), 1166–1175. https://doi.org/10.1002/j.1460-2075.1994.tb06366.x

Li, Y., Haarhuis, J. H., Sedeño Cacciatore, Á., Oldenkamp, R., van Ruiten, M. S., Willems, L., Teunissen, H., Muir, K. W., de Wit, E., Rowland, B. D., & Panne, D. (2020). The structural basis for cohesin–CTCF-anchored loops. Nature, 578(7795), 472–476. https://doi.org/10.1038/s41586-019-1910-z

Papadakis, M. A., & Workman, C. T. (2015). Oxidative stress response pathways: Fission yeast as archetype. Critical Reviews in Microbiology, 41(4), 520–535. https://doi.org/10.3109/1040841x.2013.870968

Paul, M. R., Hochwagen, A., & Ercan, S. (2018). Condensin action and compaction. Current Genetics, 65(2), 407–415. https://doi.org/10.1007/s00294-018-0899-4

Pekmez, M., Arda, N., Hamad, İ., Kiğ, C., & Temizkan, G. (2008). Hydrogen peroxide-induced oxidative damages in Schizosaccharomyces pombe. Biologia, 63(2), 151–155. https://doi.org/10.2478/s11756-008-0040-0

Petersen, J., & Russell, P. (2016). Growth and the environment of schizosaccharomyces pombe. Cold Spring Harbor Protocols, 2016(3). https://doi.org/10.1101/pdb.top079764

Pombase, the S. Pombe Genome Database. PomBase. (n.d.). https://www.pombase.org/

Potapova, T., & Gorbsky, G. (2017). The consequences of chromosome segregation errors in mitosis and meiosis. Biology, 6(4), 12. https://doi.org/10.3390/biology6010012

Seipel, K., Georgiev, O., Gerber, H., & Schaffner, W. (1993). C-Terminal Domain (CTD) of RNA-polymerase II and N-terminal segment of the human TATA binding protein (TBP) can mediate remote and proximal transcriptional activation, respectively. Nucleic Acids Research, 21(24), 5609–5615. https://doi.org/10.1093/nar/21.24.5609

Szabo, Q., Bantignies, F., & Cavalli, G. (2019). Principles of genome folding into topologically associating domains. Science Advances, 5(4). https://doi.org/10.1126/sciadv.aaw1668

Vyas, A., Freitas, A. V., Ralston, Z. A., & Tang, Z. (2021). Fission yeast schizosaccharomyces pombe: A unicellular “micromammal” model organism. Current Protocols, 1(6). https://doi.org/10.1002/cpz1.151

Wissink, E. M., Vihervaara, A., Tippens, N. D., & Lis, J. T. (2019). Nascent RNA analyses: Tracking transcription and its regulation. Nature Reviews Genetics, 20(12), 705–723. https://doi.org/10.1038/s41576-019-0159-6

Xing, H., Vanderford, N. L., & Sarge, K. D. (2008). The TBP–PP2A mitotic complex bookmarks genes by preventing condensin action. Nature Cell Biology, 10(11), 1318–1323. https://doi.org/10.1038/ncb1790

Xu, Y., Singh, A., & Alter, G. M. (2016). Hydroxyurea induces cytokinesis arrest in cells expressing a mutated sterol-14α-demethylase in the ergosterol biosynthesis pathway. Genetics, 204(3), 959–973. https://doi.org/10.1534/genetics.116.19153